Amplitude analysis of the Bs0→K#0K¯#0$$ {B}_{(s)}^0\to {K}^{\ast 0}{\overline{K}}^{\ast 0} $$ decays and measurement of the branching fraction of the B0→K#0K¯#0$ $ {B}^0\to {K}^{\ast 0}{\overline{K}}^{\ast 0} $$ decay

Amplitude analysis of the $B^0_{(s)} \to K^{*0}\overline{K}^{*0}$ decays and measurement of the branching fraction of the $B^0 \to K^{*0}\overline{K}^{*0}$ decay

The LHCb collaboration

E-mail: cibran.santamarina@usc.es

ABSTRACT: The $B^0 \to K^{*0}\overline{K}^{*0}$ and $B^0_s \to K^{*0}\overline{K}^{*0}$ decays are studied using proton-proton collision data corresponding to an integrated luminosity of $3\,\text{fb}^{-1}$. An untagged and time-integrated amplitude analysis of $B^0_{(s)} \to (K^+\pi^-)(K^-\pi^+)$ decays in two-body invariant mass regions of $150\,\text{MeV}/c^2$ around the K^{*0} mass is performed. A stronger longitudinal polarisation fraction in the $B^0 \to K^{*0}\overline{K}^{*0}$ decay, $f_L = 0.724 \pm 0.051\,(\text{stat}) \pm 0.016\,(\text{syst})$, is observed as compared to $f_L = 0.240 \pm 0.031\,(\text{stat}) \pm 0.025\,(\text{syst})$ in the $B^0_s \to K^{*0}\overline{K}^{*0}$ decay. The ratio of branching fractions of the two decays is measured and used to determine $\mathcal{B}(B^0 \to K^{*0}\overline{K}^{*0}) = (8.0 \pm 0.9\,(\text{stat}) \pm 0.4\,(\text{syst})) \times 10^{-7}$.

https://doi.org/10.1007/JHEP07(2019)032

Contents

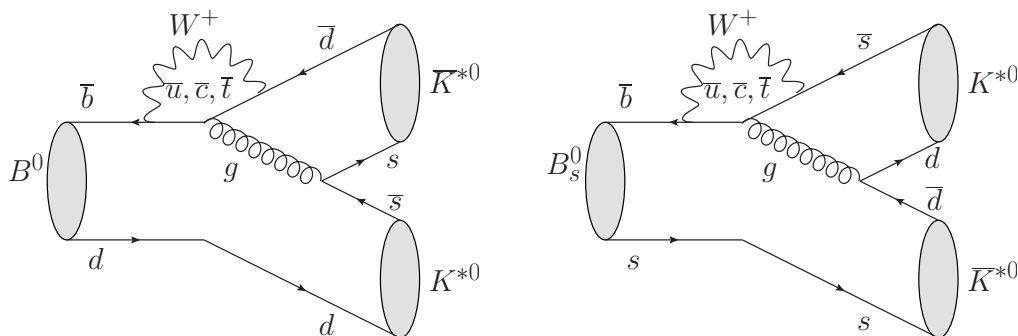## 1 Introduction

The $B^0 \to K^{*0}\overline{K}^{*0}$ decay is a Flavour-Changing Neutral Current (FCNC) process.[1] In the Standard Model (SM) this type of processes is forbidden at tree level and occurs at first order through loop penguin diagrams. Hence, FCNC processes are considered to be excellent probes for physics beyond the SM, since contributions mediated by heavy particles, contemplated in these theories, may produce effects measurable with the current sensitivity.

Evidence of the $B^0 \to K^{*0}\overline{K}^{*0}$ decay has been found by the BaBar collaboration [1] with a measured yield of $33.5^{+9.1}_{-8.1}$ decays. An untagged time-integrated analysis was presented finding a branching fraction of $\mathcal{B} = (1.28^{+0.35}_{-0.30} \pm 0.11) \times 10^{-6}$ and a longitudinal polarisation fraction of $f_L = 0.80^{+0.11}_{-0.12} \pm 0.06$. In untagged time-integrated analyses the distributions for B^0 and $\overline{B}^0$ decays are assumed to be identical and summed, so that they can be fitted with a single amplitude. However, if CP-violation effects are present, the distribution is given by the incoherent sum of the two contributions. The Belle collaboration also searched for this decay [2] and a branching fraction of $\mathcal{B} = (0.26^{+0.33+0.10}_{-0.29-0.07}) \times 10^{-6}$ was measured, disregarding S-wave contributions. There is a 2.2 standard-deviations difference between the branching fraction measured by the two experiments. The predictions

---

[1]Throughout the text charge conjugation is implied, $(K\pi)$ indicates either a $(K^+\pi^-)$ or a $(K^-\pi^+)$ pair, $B^0_{(s)}$ indicates either a B^0 or a B^0_s meson and K^{*0} refers to the $K^*(892)^0$ resonance, unless otherwise stated.

Figure 1. Leading order Feynman diagrams for the $B^0 \to K^{*0}\overline{K}^{*0}$ and $B_s^0 \to K^{*0}\overline{K}^{*0}$ decays. Both modes are dominated by a gluonic-penguin diagram.

of factorised QCD (QCDF) are $\mathcal{B} = (0.6^{+0.1+0.5}_{-0.1-0.3}) \times 10^{-6}$ and $f_L = 0.69^{+0.01+0.34}_{-0.01-0.27}$ [3]. Perturbative QCD predicts $\mathcal{B} = (0.64^{+0.24}_{-0.23}) \times 10^{-6}$ [4].[2] These theoretical predictions agree with the experimental results within the large uncertainties. The measurement of f_L agrees with the naïve hypothesis, based on the quark helicity conservation and the $V-A$ nature of the weak interaction, that charmless decays into pairs of vector mesons (VV) should be strongly longitudinally polarised. See, for example, the *Polarization in B Decays* review in ref. [5].

The $B_s^0 \to K^{*0}\overline{K}^{*0}$ decay was first observed by the LHCb experiment with early LHC data [4]. A later untagged time-integrated study, with data corresponding to $1\,\mathrm{fb}^{-1}$ of integrated luminosity, measured $\mathcal{B} = (10.8 \pm 2.1 \pm 1.5) \times 10^{-6}$ and $f_L = 0.201 \pm 0.057 \pm 0.040$ [6]. More recently, a complete CP-sensitive time-dependent analysis of $B_s^0 \to (K^+\pi^-)(K^-\pi^+)$ decays in the $(K\pi)$ mass range from 750 to $1600\,\mathrm{MeV}/c^2$ has been published by LHCb [7], with data corresponding to $3\,\mathrm{fb}^{-1}$ of integrated luminosity. A determination of $f_L = 0.208 \pm 0.032 \pm 0.046$ was performed as well as the first measurements of the mixing-induced CP-violating phase $\phi_s^{d\bar{d}}$ and of the direct CP asymmetry parameter $|\lambda|$. These LHCb analyses of $B_s^0 \to (K^+\pi^-)(K^-\pi^+)$ decays lead to three conclusions: firstly, within their uncertainties, the measured observables are compatible with the absence of CP violation; secondly, a low polarisation fraction is found; finally, a large S-wave contribution, as much as 60%, is measured in the $150\,\mathrm{MeV}/c^2$ window around the K^{*0} mass. The low longitudinal polarisation fraction shows a tension with the prediction of QCDF ($f_L = 0.63^{+0.42}_{-0.29}$ [3]) and disfavours the hypothesis of strongly longitudinally polarised VV decays. Theoretical studies try to explain the small longitudinal polarisation with mechanisms such as contributions from annihilation processes [3, 8]. It is intriguing that the two channels $B^0 \to K^{*0}\overline{K}^{*0}$ and $B_s^0 \to K^{*0}\overline{K}^{*0}$, which are related by U-spin symmetry, implying the exchange of d and s quarks as displayed in figure 1, show such different polarisations. A comprehensive theory review on polarisation of charmless VV neutral B-meson decays can be found in ref. [9].

Some authors consider the $B_s^0 \to K^{*0}\overline{K}^{*0}$ decay as a golden channel for a precision test of the CKM phase β_s [10]. High-precision analyses of this channel, dominated by the

---

[2]This reference considers two scenarios for its predictions, both giving compatible results. Only the first scenario considered therein is quoted here.

gluonic-penguin diagram, will require to account for subleading amplitudes [9, 11]. The study of the $B^0 \to K^{*0}\overline{K}^{*0}$ decay allows to control higher-order SM contributions to the $B^0_s \to K^{*0}\overline{K}^{*0}$ channel employing U-spin symmetry [10, 12]. In refs. [12, 13] more precise QCDF predictions, involving the relation between longitudinal branching fractions of the two channels, are made.

In this work, an untagged and time-integrated amplitude analysis of the $B^0 \to (K^+\pi^-)(K^-\pi^+)$ and $B^0_s \to (K^+\pi^-)(K^-\pi^+)$ decays in the two-body invariant mass regions of $150\,\mathrm{MeV}/c^2$ around the K^{*0} mass is presented, as well as the determination of the $B^0 \to K^{*0}\overline{K}^{*0}$ decay branching fraction. The analysis uses data recorded in 2011 and 2012 at centre-of-mass energies of $\sqrt{s} = 7$ and $\sqrt{s} = 8\,\mathrm{TeV}$, respectively, corresponding to an integrated luminosity of $3\,\mathrm{fb}^{-1}$.
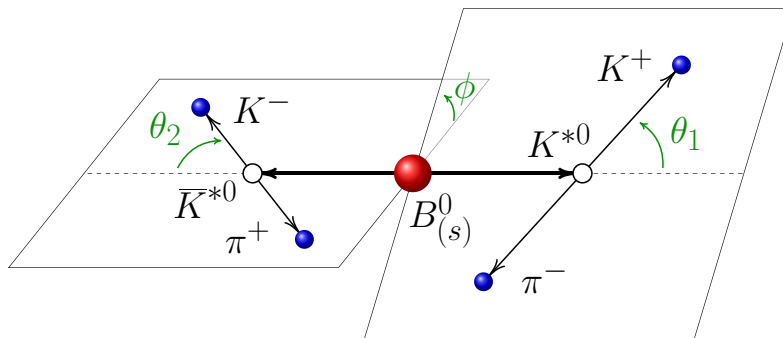
This paper is organised as follows. In section 2 the formalism of the decay amplitudes is presented. In section 3 a brief description of the LHCb detector, online selection algorithms and simulation software is given. The selection of $B^0 \to (K^+\pi^-)(K^-\pi^+)$ and $B^0_s \to (K^+\pi^-)(K^-\pi^+)$ candidates is presented in section 4. Section 5 describes the maximum-likelihood fit to the four-body invariant-mass spectra and its results. The amplitude analysis and its results are discussed in section 6. The estimation of systematic uncertainties is described in section 7, and the determination of the $B^0 \to K^{*0}\overline{K}^{*0}$ decay branching fraction relative to the $B^0_s \to K^{*0}\overline{K}^{*0}$ mode in section 8. Finally, the results are summarised and conclusions are drawn in section 9.

2 Amplitude analysis formalism

The $B^0 \to K^{*0}\overline{K}^{*0}$ and $B^0_s \to K^{*0}\overline{K}^{*0}$ modes are weak decays of a pseudoscalar particle into two vector mesons ($P \to VV$). The B-meson decays are followed by subsequent $K^{*0} \to K^+\pi^-$ and $\overline{K}^{*0} \to K^-\pi^+$ decays. The study of the angular distribution employs the helicity angles shown in figure 2: $\theta_{1(2)}$, defined as the angle between the direction of the $K^{+(-)}$ meson and the direction opposite to the B-meson momentum in the rest frame of the K^{*0} ($\overline{K}^{*0}$) resonance, and ϕ, the angle between the decay planes of the two vector mesons in the B-meson rest frame. From angular momentum conservation, three relative polarisations of the final state are possible for VV final states that correspond to longitudinal (0 or L), or transverse to the direction of motion and parallel ($\parallel$) or perpendicular ($\perp$) to each other. For the two-body invariant mass of the $(K^+\pi^-)$ and $(K^-\pi^+)$ pairs, noted as $m_1 \equiv M(K^+\pi^-)$ and $m_2 \equiv M(K^-\pi^+)$, a range of $150\,\mathrm{MeV}/c^2$ around the known K^{*0} mass [5] is considered. Therefore, $(K\pi)$ pairs may not only originate from the spin-1 K^{*0} meson, but also from other spin states. This justifies that, besides the helicity angles, a phenomenological description of the two-body invariant mass spectra, employing the isobar model, is adopted in the analytic model. In the isobar approach, the decay amplitude is modelled as a linear superposition of quasi-two-body amplitudes [14–16].

For the S-wave ($J = 0$), the $K^*_0(1430)^0$ resonance, the possible $K^*_0(700)^0$ (or κ) and a non-resonant component, $(K\pi)_0$, need to be accounted for. This is done using the LASS parameterisation [17], which is an effective-range elastic scattering amplitude, interfering with the $K^*_0(1430)^0$ meson,

$$\mathcal{M}_0(m) \propto \frac{m}{q}\left(\frac{1}{\cot\delta_\beta - i} + e^{2i\delta_\beta}\frac{M_0\Gamma_0(m)}{M_0^2 - m^2 - iM_0\Gamma_0(m)}\right), \tag{2.1}$$

Figure 2. Definition of the helicity angles, employed in the angular analysis of the $B^0_{(s)} \to K^{*0} \overline{K}^{*0}$ decays. Each angle is defined in the rest frame of the decaying particle.

where

$$\Gamma_0(m) = \Gamma_0 \frac{M_0}{m} \left(\frac{q}{q_0}\right) \tag{2.2}$$

represents the $K^*_0(1430)^0$ width. In eq. (2.1) and eq. (2.2) q is the $(K\pi)$ centre-of-mass decay momentum, and M_0, Γ_0 and q_0 are the $K^*_0(1430)^0$ mass, width and centre-of-mass decay momentum at the pole, respectively. The effective-range elastic scattering amplitude component depends on

$$\cot \delta_\beta = \frac{1}{aq} + \frac{1}{2}bq,$$

where a is the scattering length and b the effective range.

For the P-wave ($J = 1$), only the $K^*(892)^0$ resonance is considered. Other P-wave resonances, such as $K^*(1410)^0$ or $K^*(1680)^0$, with pole masses much above the fit region, are neglected. Resonances with higher spin, for instance the D-wave $K^*_2(1430)^0$ meson, are negligible in the considered two-body mass range [7] and are also disregarded. The K^{*0} amplitude is parameterised with a spin-1 relativistic Breit-Wigner amplitude,

$$\mathcal{M}_1(m) \propto \frac{m}{q} \frac{M_1 \Gamma_1(m)}{(M_1^2 - m^2) - iM_1\Gamma_1(m)}. \tag{2.3}$$

The mass-dependent width is given by

$$\Gamma_1(m) = \Gamma_1 \frac{M_1}{m} \frac{1 + r^2 q_1^2}{1 + r^2 q^2} \left(\frac{q}{q_1}\right)^3, \tag{2.4}$$

where M_1 and Γ_1 are the K^{*0} mass and width, r is the interaction radius parameterising the centrifugal barrier penetration factor, and q_1 corresponds to the centre-of-mass decay momentum at the resonance pole. The values of the mass propagator parameters are summarised in table 1.

– 4 –

	$(K\pi)_0$	K^{*0}
	$J = 0$ [17, 18]	$J = 1$ [5]
M_J [MeV/c^2]	1435 ± 7	895.81 ± 0.19
Γ_J [MeV]	279 ± 22	47.4 ± 0.6
r [c/GeV]	$-$	3.0 ± 0.5
a [c/GeV]	1.95 ± 0.11	$-$
b [c/GeV]	1.76 ± 0.76	$-$

Table 1. Parameters of the mass propagators employed in the amplitude analysis.

The differential decay rate for $B^0_{(s)}$ mesons[3] at production is given by [6, 19],

$$\frac{\mathrm{d}^5\Gamma}{\mathrm{d}\cos\theta_1\mathrm{d}\cos\theta_2\mathrm{d}\phi\mathrm{d}m_1\mathrm{d}m_2} = \frac{9}{8\pi}\Phi_4(m_1, m_2)\left|\sum_{i=1}^{6} A_i g_i(m_1, m_2, \theta_1, \theta_2, \phi)\right|^2$$

$$= \sum_{i=1}^{6}\sum_{j\geq i}^{6} \mathcal{R}e[A_i A_j^* F_{ij}], \qquad (2.5)$$

where Φ_4 is the four-body phase space factor. The index i runs over the first column of table 2 where the different decay amplitudes, $A_i \equiv |A_i|e^{i\delta_i}$, and the angular-mass functions, g_i, are listed. The angular dependence of these functions is obtained from spherical harmonics as explained in ref. [19]. For CP-studies, the CP-odd, A_S^+, and CP-even, A_S^-, eigenstates of the S-wave polarisation amplitudes are preferred to the vector-scalar (VS) and scalar-vector (SV) helicity amplitudes, to which they are related by

$$A_S^+ = \frac{A_{VS} + A_{SV}}{\sqrt{2}} \quad \text{and} \quad A_S^- = \frac{A_{VS} - A_{SV}}{\sqrt{2}}.$$

The remaining amplitudes, except for $A_\perp$, correspond to CP-even eigenstates. The contributions can be quantified by the terms F_{ij}, defined as

$$F_{ij} = \frac{9}{8\pi}\Phi_4(m_1, m_2)g_i(m_1, m_2, \theta_1, \theta_2, \phi)g_j^*(m_1, m_2, \theta_1, \theta_2, \phi)(2 - \delta_{ij}), \qquad (2.6)$$

which are normalised according to

$$\int F_{ij}\mathrm{d}m_1\mathrm{d}m_2\mathrm{d}\cos\theta_1\mathrm{d}\cos\theta_1\mathrm{d}\phi = \delta_{ij}.$$

This condition ensures that $\sum_{i=1}^{6}|A_i|^2 = 1$.

The polarisation fractions of the VV amplitudes are defined as

$$f_{L,\|,\perp} = \frac{|A_{0,\|,\perp}|^2}{|A_0|^2 + |A_\||^2 + |A_\perp|^2},$$

---

[3]Charge conjugation is not implied in the rest of this section. For the charge-conjugated mode, $\bar{B}^0_{(s)} \to (K^+\pi^-)(K^-\pi^+)$, the decay rate is obtained applying the transformation $A_i \to \eta_i \bar{A}_i$ in eq. (2.5) where the corresponding CP eigenvalues, η_i, are given in table 2.

i	A_i	η_i	$g_i(m_1, m_2, \theta_1, \theta_2, \phi)$
1	A_0	1	$\cos\theta_1 \cos\theta_2 \mathcal{M}_1(m_1)\mathcal{M}_1(m_2)$
2	$A_\parallel$	1	$\frac{1}{\sqrt{2}}\sin\theta_1\sin\theta_2\cos\phi\,\mathcal{M}_1(m_1)\mathcal{M}_1(m_2)$
3	$A_\perp$	-1	$\frac{i}{\sqrt{2}}\sin\theta_1\sin\theta_2\sin\phi\,\mathcal{M}_1(m_1)\mathcal{M}_1(m_2)$
4	A_S^+	-1	$-\frac{1}{\sqrt{6}}(\cos\theta_1\mathcal{M}_1(m_1)\mathcal{M}_0(m_2) - \cos\theta_2\mathcal{M}_0(m_1)\mathcal{M}_1(m_2))$
5	A_S^-	1	$-\frac{1}{\sqrt{6}}(\cos\theta_1\mathcal{M}_1(m_1)\mathcal{M}_0(m_2) + \cos\theta_2\mathcal{M}_0(m_1)\mathcal{M}_1(m_2))$
6	A_{SS}	1	$-\frac{1}{3}\mathcal{M}_0(m_1)\mathcal{M}_0(m_2)$

Table 2. Amplitudes, A_i, and angle-mass functions, $g_i(m_1, m_2, \theta_1, \theta_2, \phi)$, of the differential decay rate of eq. (2.5). In particular, A_0, $A_\parallel$ and $A_\perp$ are the longitudinal, parallel and transverse helicity amplitudes of the P-wave whereas A_S^+ and A_S^- are the combinations of CP eigenstate amplitudes of the SV and VS states and A_{SS} is the double S-wave amplitude. The table indicates the corresponding CP eigenvalue, η_i. The mass propagators, $\mathcal{M}_{0,1}(m)$, are discussed in the text.

where A_0, $A_\parallel$ and $A_\perp$ are the longitudinal, parallel and transverse amplitudes of the P-wave. Therefore, f_L is the fraction of $B_{(s)}^0 \to K^{*0}\overline{K}^{*0}$ longitudinally polarised decays. The polarisation fractions are preferred to the amplitude moduli since they are independent of the considered $(K\pi)$ mass range. The P-wave amplitudes moduli can always be recovered as

$$|A_{0,\parallel,\perp}|^2 = (1 - |A_S^+|^2 - |A_S^-|^2 - |A_{SS}|^2)\,f_{L,\parallel,\perp}.$$

The phase of all propagators is set to be zero at the K^{*0} mass. In addition, a global phase can be factorised without affecting the decay rate setting $\delta_0 \equiv 0$. The last two requirements establish the definition of the amplitude phases ($\delta_\parallel$, $\delta_\perp$, δ_S^-, δ_S^+ and δ_{SS}) as the phase relative to that of the longitudinal P-wave amplitude at the K^{*0} mass.

Since $B_{(s)}^0$ mesons oscillate, the decay rate evolves with time. The time-dependent amplitudes are obtained replacing $A_i \to \mathcal{A}_i(t)$ and $\bar{A}_i \to \bar{\mathcal{A}}_i(t)$ in eq. (2.5) being

$$\mathcal{A}_i(t) = \left[g_+(t)A_i + \eta_i\frac{\mathrm{q}}{\mathrm{p}}g_-(t)\bar{A}_i\right] \quad \text{and} \quad \bar{\mathcal{A}}_i(t) = \left[\frac{\mathrm{p}}{\mathrm{q}}g_-(t)A_i + \eta_i g_+(t)\bar{A}_i\right],$$

with

$$g_+(t) = \frac{1}{2}\left(e^{-\left(iM_{\mathrm{L}}+\frac{\Gamma_{\mathrm{L}}}{2}\right)t} + e^{-\left(iM_{\mathrm{H}}+\frac{\Gamma_{\mathrm{H}}}{2}\right)t}\right)$$

$$\text{and} \quad g_-(t) = \frac{1}{2}\left(e^{-\left(iM_{\mathrm{L}}+\frac{\Gamma_{\mathrm{L}}}{2}\right)t} - e^{-\left(iM_{\mathrm{H}}+\frac{\Gamma_{\mathrm{H}}}{2}\right)t}\right),$$

where Γ_{L} and Γ_{H} are the widths of the light and heavy mass eigenstates of the $B_{(s)}^0 - \overline{B}_{(s)}^0$ system and M_{L} and M_{H} are their masses. The coefficients p and q are the mixing terms that relate the flavour and mass eigenstates,

$$B_{(s)\mathrm{H}}^0 = \mathrm{p}B_{(s)}^0 + \mathrm{q}\overline{B}_{(s)}^0 \quad \text{and} \quad B_{(s)\mathrm{L}}^0 = \mathrm{p}B_{(s)}^0 - \mathrm{q}\overline{B}_{(s)}^0.$$

Masses and widths are often considered in their averages and differences, $M = (M_{\mathrm{L}} + M_{\mathrm{H}})/2$, $\Delta M = M_{\mathrm{L}} - M_{\mathrm{H}}$, $\Gamma = (\Gamma_{\mathrm{L}} + \Gamma_{\mathrm{H}})/2$ and $\Delta\Gamma = \Gamma_{\mathrm{L}} - \Gamma_{\mathrm{H}}$, in

particular in their relation with the mixing phase,

$$\tan \phi_{(s)} = 2\frac{\Delta M}{\Delta \Gamma}\left(1 - \frac{|\mathrm{q}|}{|\mathrm{p}|}\right). \tag{2.7}$$

In this analysis, no attempt is made to identify the flavour of the initial $B^0_{(s)}$ meson and time-integrated spectra are considered. Consequently, the selected candidates correspond to untagged and time-integrated decay rates and there is no sensitivity to direct and mixing-induced CP violation. Moreover, since the origin of phases is set in a CP-even eigenstate ($\delta_0 = 0$), for the CP-odd eigenstates, the untagged time-integrated decay is only sensitive to the phase difference $\delta_\perp - \delta_S^+$. The present experimental knowledge is compatible with small CP violation in mixing [20] and with the absence of direct CP violation in the $B^0_s \to (K^+\pi^-)(K^-\pi^+)$ system [7].

The dependence of the decay rate in an untagged and time-integrated analysis of a $B^0_{(s)}$ meson can be expressed as

$$\frac{\mathrm{d}^5(\Gamma + \overline{\Gamma})}{\mathrm{d}\cos\theta_1\,\mathrm{d}\cos\theta_2\,\mathrm{d}\phi\,\mathrm{d}m_1\,\mathrm{d}m_2} = N\sum_{i=1}^{6}\sum_{j\geq i}^{6}\mathcal{R}e\left[A_i A_j^*\left(\frac{1-\eta_i}{\Gamma_{\mathrm{H}}} + \frac{1+\eta_i}{\Gamma_{\mathrm{L}}}\right)F_{ij}\delta_{\eta_i\eta_j}\right], \tag{2.8}$$

where the A_i amplitudes account for the the average of $B^0_{(s)}$ and $\overline{B}^0_{(s)}$ decays and N is a normalisation constant. For the B^0 meson, a further simplification of the decay rate is considered, since $\Delta\Gamma/\Gamma = -0.002 \pm 0.010$ [20] the light and heavy mass eigenstate widths can be assumed to be equal,

$$\left(\frac{1-\eta_i}{\Gamma_{\mathrm{H}}} + \frac{1+\eta_i}{\Gamma_{\mathrm{L}}}\right) \approx \frac{2}{\Gamma},$$

and this factor can be extracted as part of the normalisation constant in eq. (2.8). For the B^0_s meson the central values $\Gamma_{\mathrm{H}} = 0.618\,\mathrm{ps}^{-1}$ and $\Gamma_{\mathrm{L}} = 0.708\,\mathrm{ps}^{-1}$ [20] are considered.

3 Detector and simulation

The LHCb detector [21, 22] is a single-arm forward spectrometer covering the pseudorapidity range $2 < \eta < 5$, designed for the study of particles containing b or c quarks. The detector includes a high-precision tracking system consisting of a silicon-strip vertex detector surrounding the pp interaction region, a large-area silicon-strip detector located upstream of a dipole magnet with a bending power of about $4\,\mathrm{Tm}$, and three stations of silicon-strip detectors and straw drift tubes placed downstream of the magnet. The tracking system provides a measurement of the momentum, p, of charged particles with a relative uncertainty that varies from 0.5% at low momentum to 1.0% at $200\,\mathrm{GeV}/c$. The minimum distance of a track to a primary vertex (PV), the impact parameter (IP), is measured with a resolution of $(15 + 29/p_{\mathrm{T}})\,\mu\mathrm{m}$, where p_{T} is the component of the momentum transverse to the beam, in GeV/c. Different types of charged hadrons are distinguished using information from two ring-imaging Cherenkov detectors. Photons, electrons and hadrons are identified by a calorimeter system consisting of scintillating-pad and preshower detectors,

an electromagnetic and a hadronic calorimeter. Muons are identified by a system composed of alternating layers of iron and multiwire proportional chambers.

The magnetic field deflects oppositely charged particles in opposite directions and this can lead to detection asymmetries. Periodically reversing the magnetic field polarity throughout the data-taking almost cancels the effect. The configuration with the magnetic field pointing upwards (downwards), *MagUp* (*MagDown*), bends positively (negatively) charged particles in the horizontal plane towards the centre of the LHC ring.

The online event selection is performed by a trigger [23], which consists of a hardware stage, based on information from the calorimeter and muon systems, followed by a software stage, which applies a full event reconstruction. In the offline selection, trigger signatures are associated with reconstructed particles. Since the trigger system uses the p_{T} of the charged particles, the phase-space and time acceptance is different for events where signal tracks were involved in the trigger decision (called trigger-on-signal or TOS throughout) and those where the trigger decision was made using information from the rest of the event only (noTOS).

Simulated samples of the $B^0 \to K^{*0} \overline{K}^{*0}$ and $B^0_s \to K^{*0} \overline{K}^{*0}$ decays with longitudinal polarisation fractions of 0.81 and 0.64, respectively, are primarily employed in these analyses, particularly for the acceptance description as explained in section 6. Simulated samples of the main peaking background contributions, $B^0 \to K^{*0} \phi(K^+ K^-)$, $B^0 \to \rho^0 K^{*0}$ and $\Lambda_b^0 \to K^{*0} p \pi^-$, are also considered. In the simulation, pp collisions are generated using PYTHIA [24] with a specific LHCb configuration [25]. Decays of hadronic particles are described by EVTGEN [26], in which final-state radiation is generated using PHOTOS [27]. The interaction of the generated particles with the detector, and its response, are implemented using the GEANT4 toolkit [28, 29] as described in ref. [30].

4 Signal selection

Both data and simulation are filtered with a preliminary selection. Events containing four good quality tracks with $p_{\mathrm{T}} > 500\,\mathrm{MeV}/c$ are retained. In events that contain more than one PV, the $B^0_{(s)}$ candidate constructed with these four tracks is associated with the PV that has the smallest χ^2_{IP}, where χ^2_{IP} is defined as the difference in the vertex-fit χ^2 of the PV reconstructed with and without the track or tracks in question. Each of the four tracks must fulfil $\chi^2_{\mathrm{IP}} > 9$ with respect to the PV and originate from a common vertex of good quality ($\chi^2/\mathrm{ndf} < 15$, where ndf is the number of degrees of freedom of the vertex). To identify kaons and pions, a selection in the difference of the log-likelihoods of the kaon and pion hypothesis ($\mathrm{DLL}_{K\pi}$) is applied. This selection is complemented with fiducial constraints that optimise the particle identification determination: the pion and kaon candidates are required to have $3 < p < 100\,\mathrm{GeV}/c$ and $1.5 < \eta < 4.5$ and be inconsistent with muon hypothesis. The final state opposite charge ($K\pi$) pairs are combined into K^{*0} and $\overline{K}^{*0}$ candidates with a mass within $150\,\mathrm{MeV}/c^2$ of the K^{*0} mass. The K^{*0} and $\overline{K}^{*0}$ candidates must have $p_{\mathrm{T}} > 900\,\mathrm{MeV}/c$ and vertex $\chi^2/\mathrm{ndf} < 9$. The intermediate resonances must combine into $B^0_{(s)}$ candidates within $500\,\mathrm{MeV}/c^2$ of the B^0_s mass, with a distance of closest approach between their trajectories of less than $0.3\,\mathrm{mm}$.

To guarantee that the $B^0_{(s)}$ candidate originates in the interaction point, the cosine of the angle between the $B^0_{(s)}$ momentum and the direction of flight from the PV to the decay vertex is required to be larger than 0.99 and the χ^2_{IP} with respect to the PV has to be smaller than 25.

A multivariate selection based on a Boosted Decision Tree with Gradient Boost [31, 32] (BDTG) is employed. It relies on the aforementioned variables and on the $B^0_{(s)}$ candidate flight distance with respect to the PV and its p_{T}. Simulated $B^0 \to K^{*0}\overline{K}^{*0}$ decays with tracks matched to the generator particles and filtered with the preliminary selection are used as signal sample, whereas the four-body invariant-mass sideband $5600 < M(K^+\pi^-K^-\pi^+) < 5800\,\text{MeV}/c^2$, composed of purely combinatorial $(K^+\pi^-)(K^-\pi^+)$ combinations, is used as background sample for the BDTG training. The number of events in the signal training sample of the BDTG is determined using the ratio between the B^0_s and the B^0 yields from ref. [6] and the B^0_s yield obtained with a four-body mass fit to the data sample after the preliminary selection. The number of events in the background training sample of the BDTG is estimated by extrapolating the background yield in the sideband into the $\pm 30\,\text{MeV}/c^2$ window around the B^0 mass. The requirement on the BDTG output is chosen to maximise the figure of merit $N_S/\sqrt{N_S + N_B}$, where N_S and N_B are the expected output signal and background yields, respectively. Different BDTGs are implemented for 2011 and 2012 data.

A comprehensive search for peaking backgrounds, mainly involving intermediate charm particles, is performed. Decays of B mesons sharing the same final state with the signal,[4] such as $B^0 \to D^0(K^+K^-)\pi^+\pi^-$ ($\mathcal{B} \sim 3\times 10^{-6}$) and $B^0 \to D^0(\pi^+\pi^-)K^+K^-$ ($\mathcal{B} \sim 6\times 10^{-8}$) decays, are strongly suppressed by the requirement in the $(K\pi)$ mass. Resonances in three-body combinations $(K^+K^-\pi^+)$ and $(K^+\pi^+\pi^-)$ are also explored. In the case of the former, the three-body invariant mass in the data sample is above all known charm resonances. For the latter, no evidence of candidates originated in $B^0 \to D^{\mp}K^{\pm}$ and $B^0 \to D_s^{\mp}K^{\pm}$ decays ($\mathcal{B} \sim 10^{-7}$) or in $B^0_s \to D_s^{\mp}K^{\pm}$ decays ($\mathcal{B} \sim 10^{-6}$) is found. Three-body combinations with a pion misidentified as a kaon are reconstructed, mainly searching for $B^0 \to D^-(\pi^-\pi^-K^+)\pi^+$ decays ($\mathcal{B} = 2.45 \times 10^{-4}$), but also for $B^0_s \to D_s^{\pm}K^{\mp}$ ($\mathcal{B} \sim 10^{-5}$), $B^0 \to D^-K^+$ and $B^0 \to D_s^-K^+$ ($\mathcal{B} \sim 10^{-6}$) decays. All of them are suppressed to a negligible level by the applied selection. A search of three-body combinations with a proton misidentified as a kaon is performed, finding no relevant contribution from decays involving a Λ_c^+ baryon. Decays into five final-state particles are also investigated. Contributions of the $B^0 \to \eta'(\gamma\pi^+\pi^-)K^{*0}$ decay can be neglected due to the small misidentification probability and the four-body mass distribution whereas the $B^0_s \to \phi(\pi^0\pi^+\pi^-)\phi(K^+K^-)$ decay is negligible due to the requirement on the $(K\pi)$ mass.
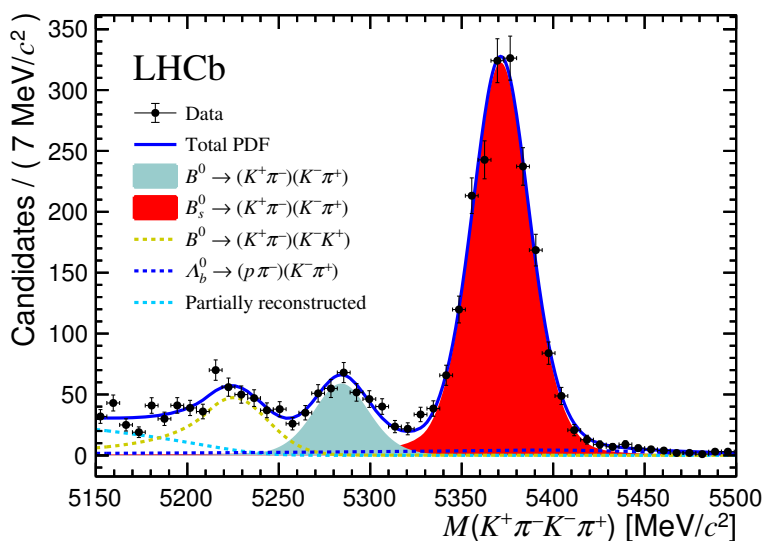
5 Four-body mass spectrum

The signal and background yields are determined by means of a simultaneous extended maximum-likelihood fit to the invariant-mass spectra of the four final-state particles in the 2011 and 2012 data samples. The $B^0_{(s)} \to (K^+\pi^-)(K^-\pi^+)$ signal decays are parameterised

---

[4]The branching fractions in this section are taken from ref. [5].

with double-sided Hypatia distributions [33] with the same parameters except for their means that are shifted by the difference between the B^0 and B_s^0 masses, $87.13\,\mathrm{MeV}/c^2$ [5]. Misidentified $B^0 \to (K^+\pi^-)(K^-K^+)$ (including $B^0 \to K^{*0}\phi$ decays), $\Lambda_b^0 \to (p\pi^-)(K^+\pi^-)$ and $B^0 \to \rho^0 K^{*0}$ decays are also considered in the fit. Both the $B^0 \to (K^+\pi^-)(K^-K^+)$ and $\Lambda_b^0 \to (p\pi^-)(K^-\pi^+)$ contributions are described with the sum of a Crystal Ball [34] function and a Gaussian distribution which shares mean with the Crystal Ball core. The parameters of these distributions are obtained from simulation, apart from the mean and resolution values which are free to vary in the fit. Whereas the distribution mean values are constrained to be the same in the 2011 and 2012 data, the resolution is allowed to have different values for the two samples. The small contributions from $B^0 \to \rho^0 K^{*0}$ and $\Lambda_b^0 \to (p\pi^-)(K^-\pi^+)$ decays have a broad distribution in the four-body mass and are the object of specific treatment. The contribution from $B^0 \to \rho^0 K^{*0}$ decays has an expected yield of 3.5 ± 1.3 (6.6 ± 2.3) in the 2011 (2012) sample. It is estimated from the detection and selection efficiency measured with simulation, the collected luminosities, the cross section for $b\bar{b}$ production, the hadronisation fractions of B^0 and B_s^0 mesons and the known branching fraction of the mode. Simulated events containing this decay mode are added with negative weights to the final data sample to subtract its contribution. The contribution of $\Lambda_b^0 \to (p\pi^-)(K^-\pi^+)$ decays in the 2011 (2012) sample is determined to be 36 ± 16 (120 ± 28) from a fit to the $(p\pi^-K^-\pi^+)$ four-body mass spectrum of the selected data. In this study the four-body invariant mass is recomputed assigning the proton mass to the kaon with the largest DLL_{pK} value. In these fits the Λ_b^0 component is described with a Gaussian distribution and the dominant $B_s^0 \to (K^+\pi^-)(K^-\pi^+)$ background is described with a Crystal Ball function. The parameters of both lineshapes are obtained from simulation. The remaining contributions, mainly $B^0 \to (K^+\pi^-)(K^-K^+)$ and partially reconstructed events, are parameterised with a decreasing exponential with a free decay constant. The $\Lambda_b^0 \to (p\pi^-)(K^-\pi^+)$ decay angular distribution is currently unknown and its contribution can not be subtracted with negatively weighted simulated events. Its subtraction is commented further below.

Finally, contributions from partially reconstructed b-hadron decays and combinatorial background are also considered. The former is composed of B- and B_s^0-meson decays containing neutral particles that are not reconstructed. Because of the missing particle, the measured four-body invariant mass of these candidates lies in the lower sideband of the spectrum. All contributions to this background are jointly parameterised with an ARGUS function [35] convolved with a Gaussian resolution function, with the same width as the signal. The endpoint of the distribution is also fixed to the B_s^0 mass minus the π^0 mass. The combinatorial background is composed of charged tracks that are not originating from the signal decay chain. It is modelled with a linear distribution, with a free slope parameter, separate for 2011 and 2012 data samples.

The results of the fit to the four-body mass spectrum are shown in figure 3 and the yields are reported in table 3. In total, about three hundred $B^0 \to (K^+\pi^-)(K^-\pi^+)$ signal candidates are found, a factor seven larger than previous analyses [1, 2]. To perform a background-subtracted amplitude analysis, the *sPlot* technique [36, 37] is applied to isolate either the $B^0 \to (K^+\pi^-)(K^-\pi^+)$ or the $B_s^0 \to (K^+\pi^-)(K^-\pi^+)$ decays. The contribution

Figure 3. Aggregated four-body invariant-mass fit result of the 2011 and 2012 data. The solid red distribution corresponds to the $B_s^0 \to (K^+\pi^-)(K^-\pi^+)$ decay, the solid cyan distribution to $B^0 \to (K^+\pi^-)(K^-\pi^+)$, the dotted dark blue line to $\Lambda_b^0 \to (p\pi^-)(K^-\pi^+)$, the dotted yellow line to $B^0 \to (K^+\pi^-)(K^-K^+)$ and the dotted cyan line represents the partially reconstructed background. The tiny combinatorial background contribution is not represented. The black points with error bars correspond to data to which the $B^0 \to \rho^0 K^{*0}$ contribution has been subtracted with negatively weighted simulation, and the overall fit is represented by the thick blue line.

Yield	2011 sample	2012 sample
$B^0 \to (K^+\pi^-)(K^-\pi^+)$	$99 \pm 12 \pm 3$	$249 \pm 19 \pm 5$
$B_s^0 \to (K^+\pi^-)(K^-\pi^+)$	$617 \pm 26 \pm 8$	$1337 \pm 39 \pm 12$
Misidentified $B^0 \to (K^+\pi^-)(K^-K^+)$	$145 \pm 17 \pm 2$	$266 \pm 27 \pm 8$
Partially reconstructed background	$100 \pm 15 \pm 4$	$230 \pm 25 \pm 6$
Combinatorial background	$7 \pm 5 \pm 11$	$48 \pm 25 \pm 25$

Table 3. Signal and background yields for the 2011 and 2012 data samples, obtained from the fit to the four-body mass spectrum of the selected candidates. Statistical and systematic uncertainties are reported, the latter are estimated as explained in section 8.

from $\Lambda_b^0 \to (p\pi^-)(K^-\pi^+)$, for which the yield is fixed, is treated using extended weights according to appendix B.2 of ref. [36]. The *sPlot* method suppresses the background contributions using their relative abundance in the four-body invariant mass spectrum and, therefore, no assumption is required for their phase-space distribution.

6 Amplitude analysis

Each of the background-subtracted samples of $B^0 \to (K^+\pi^-)(K^-\pi^+)$ and $B_s^0 \to (K^+\pi^-)(K^-\pi^+)$ decays is the object of a separate amplitude analysis based on the model described in section 2. As a first step, the effect of a non-uniform efficiency,

depending on the helicity angles and the two-body invariant masses, is examined. For this purpose, four categories are defined according to the hardware trigger decisions (TOS or noTOS) and data-taking period (2011 and 2012). The efficiency is accounted for through the complex integrals [38]

$$\omega_{ij}^k = \int \varepsilon(m_1, m_2, \theta_1, \theta_2, \phi) F_{ij} \mathrm{d}m_1 \mathrm{d}m_2 \mathrm{d}\cos\theta_1 \mathrm{d}\cos\theta_2 \mathrm{d}\phi, \tag{6.1}$$

where ε is the total phase-space dependent efficiency, k is the sample category and F_{ij} are defined in eq. (2.6). The integrals of eq. (6.1) are determined using simulated signal samples of each of the four categories, selected with the same criteria applied to data. A single set of integrals is used for both the B_s^0 and the B^0 amplitude analyses. A probability density function (PDF) for each category is built

$$S^k(m_1, m_2, \theta_1, \theta_2, \phi) = \frac{\sum\limits_{i=1}^{6}\sum\limits_{j \geq i}^{6} \mathcal{R}e\left[A_i A_j^* \left(\frac{1-\eta_i}{\Gamma_H} + \frac{1+\eta_i}{\Gamma_L}\right) F_{ij} \delta_{\eta_i \eta_j}\right]}{\sum\limits_{i=1}^{6}\sum\limits_{j \geq i}^{6} \mathcal{R}e\left[A_i A_j^* \left(\frac{1-\eta_i}{\Gamma_H} + \frac{1+\eta_i}{\Gamma_L}\right) \omega_{ij}^k \delta_{\eta_i \eta_j}\right]}, \tag{6.2}$$

where A_i and η_i are given in table 2.

Candidates from all categories are processed in a simultaneous unbinned maximum-likelihood fit, separately for each signal decay mode, using the PDFs in eq. (6.2). To avoid nonphysical values of the parameters during the minimisation, some of them are redefined as

$$f_{\parallel} = x_{f_{\parallel}}(1 - f_L),$$
$$f_{\perp} = (1 - x_{f_{\parallel}})(1 - f_L),$$
$$|A_S^+|^2 = x_{|A_S^+|^2}(1 - |A_S^-|^2),$$
$$|A_{SS}|^2 = x_{|A_{SS}|^2}(1 - |A_S^-|^2 - |A_S^+|^2),$$

where $x_{f_{\parallel}}$, $x_{|A_S^+|^2}$ and $x_{|A_{SS}|^2}$ are used in the fit, together with f_L, $|A_S^-|^2$, $\delta_{\parallel}$, $\delta_{\perp} - \delta_S^+$, δ_S^- and δ_{SS}. The former three variables are free to vary within the range $[0, 1]$, ensuring that the sum of all the squared amplitudes is never greater than 1. The fit results are corrected for a small reducible bias, originated in discrepancies between data and simulation, as explained in section 7. The final results are shown in table 4.

Figures 4 and 5 show the one-dimensional projections of the amplitude fit to the $B^0 \to (K^+\pi^-)(K^-\pi^+)$ and $B_s^0 \to (K^+\pi^-)(K^-\pi^+)$ signal samples in which the background is statistically subtracted by means of the *sPlot* technique. Three contributions are shown: VV, produced by $(K^+\pi^-)$ $(K^-\pi^+)$ pairs originating in a $K^{*0}\overline{K}^{*0}$ decay; VS, accounting for amplitudes in which only one of the $(K\pi)$ pairs originates in a K^{*0} decay; and SS, where none of the two $(K\pi)$ pairs originate in a K^{*0} decay.

The fraction of VV decays, or purity at production, of the $B^0 \to K^{*0}\overline{K}^{*0}$ signal, $f_{B^0}^P$, is estimated from the amplitude analysis and found to be

$$f_{B^0}^P \equiv 1 - |A_{SS}|^2 - |A_S^+|^2 - |A_S^-|^2 = 0.592 \pm 0.050\,(\text{stat}) \pm 0.017\,(\text{syst}).$$

Parameter	$B^0 \to K^{*0}\overline{K}^{*0}$	$B_s^0 \to K^{*0}\overline{K}^{*0}$
f_L	$0.724 \pm 0.051 \pm 0.016$	$0.240 \pm 0.031 \pm 0.025$
$x_{f_\parallel}$	$0.42 \pm 0.10 \pm 0.03$	$0.307 \pm 0.031 \pm 0.010$
$|A_S^-|^2$	$0.377 \pm 0.052 \pm 0.024$	$0.558 \pm 0.021 \pm 0.014$
$x_{|A_S^+|^2}$	$0.013 \pm 0.027 \pm 0.011$	$0.109 \pm 0.028 \pm 0.024$
$x_{|A_{SS}|^2}$	$0.038 \pm 0.022 \pm 0.006$	$0.222 \pm 0.025 \pm 0.031$
$\delta_\parallel$	$2.51 \pm 0.22 \pm 0.06$	$2.37 \pm 0.12 \pm 0.06$
$\delta_\perp - \delta_S^+$	$5.44 \pm 0.86 \pm 0.22$	$4.40 \pm 0.17 \pm 0.07$
δ_S^-	$5.11 \pm 0.13 \pm 0.04$	$1.80 \pm 0.10 \pm 0.06$
δ_{SS}	$2.88 \pm 0.35 \pm 0.13$	$0.99 \pm 0.13 \pm 0.06$
$f_\parallel$	$0.116 \pm 0.033 \pm 0.012$	$0.234 \pm 0.025 \pm 0.010$
$f_\perp$	$0.160 \pm 0.044 \pm 0.012$	$0.526 \pm 0.032 \pm 0.019$
$|A_S^+|^2$	$0.008 \pm 0.013 \pm 0.007$	$0.048 \pm 0.014 \pm 0.011$
$|A_{SS}|^2$	$0.023 \pm 0.014 \pm 0.004$	$0.087 \pm 0.011 \pm 0.011$
S-wave fraction	$0.408 \pm 0.050 \pm 0.017$	$0.694 \pm 0.016 \pm 0.010$

Table 4. Results of the amplitude analysis of $B^0 \to (K^+\pi^-)(K^-\pi^+)$ and $B_s^0 \to (K^+\pi^-)(K^-\pi^+)$ decays. The observables above the line are directly obtained from the maximum-likelihood fit whereas those below are obtained from the former, as explained in the text, with correlations accounted for in their estimated uncertainties. For each result, the first quoted uncertainty is statistical and the second systematic. The estimation of the latter is described in section 7.

The significance of this magnitude, computed as its value over the sum in quadrature of the statistical and systematic uncertainty, is found to be 10.8 standard deviations. This significance corresponds to the presence of $B^0 \to K^{*0}\overline{K}^{*0}$ VV decays in the data sample. The S-wave fraction of the decay is equal to $0.408 = 1 - f_{B^0}^P$. For the $B_s^0 \to K^{*0}\overline{K}^{*0}$ mode the S-wave fraction is found to be $0.694 \pm 0.016\,(\text{stat}) \pm 0.010\,(\text{syst})$.

7 Systematic uncertainties of the amplitude analysis

Several sources of systematic uncertainty that affect the results of the amplitude analysis are considered and discussed in the following.

Fit method. Biases induced by the fitting method are evaluated with a large ensemble of pseudoexperiments. For each signal decay, samples with the same yield of signal observed in data (see table 3) are generated according to the PDF of eq. (2.8) with inputs set to the results summarised in table 4. The use of the weights defined in eq. (6.1) to account the detector acceptance would require a full simulation and, instead, a parametric efficiency is considered. For each observable, the mean deviation of the result from the input value is assigned as a systematic uncertainty.

Description of the kinematic acceptance. The uncertainty on the signal efficiency relies on the coefficients of eq. (6.1) that are estimated with simulation. To evaluate its impact on the amplitude analysis results, the fit to data is repeated several times

Figure 4. Projections of the amplitude fit results for the $B^0 \to K^{*0}\overline{K}^{*0}$ decay mode on the helicity angles (top row: $\cos\theta_1$ left, $\cos\theta_2$ centre and ϕ right) and on the two-body invariant masses (bottom row: $M(K^+\pi^-)$ left and $M(K^-\pi^+)$ centre). The contributing partial waves: VV (dashed red), VS (dashed green) and SS (dotted grey) are shown with lines. The black points correspond to data and the overall fit is represented by the blue line.
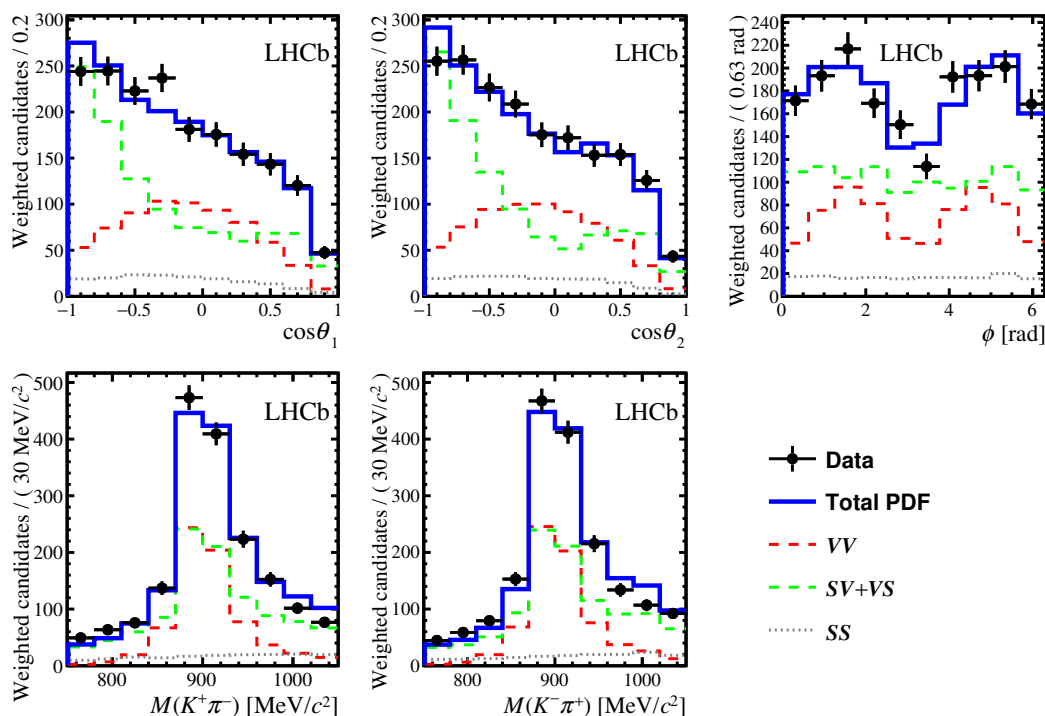
with alternative coefficients varied according to their covariance matrix. The standard deviation of the distribution of the fit results for each observable is assigned as a systematic uncertainty.

Resolution. The fit performed assumes a perfect resolution on the phase-space variables. The impact of the detector resolution on these variables is estimated with sets of pseudoexperiments adding per-event random deviations according to the resolution estimated from simulation. For each observable, the mean deviation of the result from the measured value is assigned as a systematic uncertainty.

P-wave mass model. The amplitude analysis is repeated with alternative values of the parameters that define the P-wave mass propagator, detailed in table 1, randomly sampled from their known values [5]. The standard deviation of the distribution of the amplitude fit results for each observable is assigned as a systematic uncertainty.

S-wave mass model. In addition to the default S-wave propagator, described in section 2, two alternative models are used: the LASS lineshape with the parameters of table 5, obtained with $B^0 \to J/\psi K^+\pi^-$ decays within the analysis of ref. [39], and the propagator proposed in ref. [40]. The amplitude fit is performed with these two

Figure 5. Projections of the amplitude fit results for the $B_s^0 \to K^{*0}\overline{K}^{*0}$ decay mode on the helicity angles (top row: $\cos\theta_1$ left, $\cos\theta_2$ centre and ϕ right) and on the two-body invariant masses (bottom row: $M(K^+\pi^-)$ left and $M(K^-\pi^+)$ centre). The contributing partial waves: VV (dashed red), VS (dashed green) and SS (dotted grey) are shown with lines. The black points correspond to data and the overall fit is represented by the blue line.

	$(K^+\pi^-)_0$
M_0 [MeV/c^2]	1456.7 ± 3.9
Γ_0 [MeV]	323 ± 11
a [c/GeV]	3.83 ± 0.11
b [c/GeV]	2.86 ± 0.22

Table 5. Alternative parameters of the LASS mass propagator used in the S-wave systematic uncertainty estimation.

alternatives and, for each observable, the largest deviation from the baseline result is assigned as a systematic uncertainty.

Differences between data and simulation. An iterative method [41], is used to weight the simulated events and improve the description of the track multiplicity and $B_{(s)}^0$-meson momentum distributions. The procedure is repeated multiple times and, for each observable, the mean bias of the amplitude fit result is corrected for in the results of table 4 while its standard deviation is assigned as a systematic uncertainty.

Background subtraction. The data set used in the amplitude analysis is background subtracted using the *sPlot* method [36, 37] that relies in the lineshapes of the four-

body mass fit discussed in section 5. The uncertainty related to the determination of the signal weights is evaluated repeating the amplitude analysis fits with weights obtained fitting the four-body invariant-mass with two alternative models. In the first case, the model describing the signal is defined by the sum of two Crystal Ball functions [34] with a common, free, peak value and the resolution parameter fixed from simulation. In the second case, the model describing the combinatorial background is assumed to be an exponential function. The amplitude fit is performed with the *sPlot*-weights obtained with the two alternatives and, for each observable, the largest deviation from the baseline result is assigned as a systematic uncertainty. This procedure is also used when addressing the systematic uncertainties in the measured yields of the different subsamples, as discussed in section 8.

Peaking backgrounds. The uncertainty related to the fluctuations in the yields of the $\Lambda_b^0 \to (p\pi^-)(K^-\pi^+)$ and $B^0 \to \rho^0 K^{*0}$ background contributions are estimated repeating the amplitude-analysis fit with the yield values varied by their uncertainties reported in section 5. For each observable, the largest deviation from the default result is assigned as a systematic uncertainty. This procedure is also used when addressing the systematic uncertainties of the four-body invariant mass yields in section 8.

Time acceptance. The amplitude analysis does not account for possible decay-time dependency of the efficiency, however, the trigger and the offline selections may have an impact on it. This effect only affects B_s^0-meson decays and is accounted for by estimating effective shifts: $\Gamma_{\mathrm{H}} = 0.618 \to 0.598 \, \mathrm{ps}^{-1}$ and $\Gamma_{\mathrm{L}} = 0.708 \to 0.732 \, \mathrm{ps}^{-1}$, which are obtained with simulation. For each observable, the variation of the result of the fit after introducing these values in the amplitude analysis is considered as a systematic uncertainty.

The resulting systematic uncertainties and the corrected biases, originated in the differences between data and simulation, are detailed in table 6 for the parameters of the amplitude-analysis fit. The corresponding values for the derived observables are summarised in table 7. The total systematic uncertainty is computed as the sum in quadrature of the different contributions.

8 Determination of the ratio of branching fractions

In this analysis, the $B^0 \to K^{*0}\overline{K}^{*0}$ branching fraction is measured relative to that of $B_s^0 \to K^{*0}\overline{K}^{*0}$ decays. Since both decays are selected in the same data sample and share a common final state most systematic effects cancel. However, some efficiency corrections, eg. those originated from the difference in phase-space distributions of events of the two modes, need to be accounted for. The amplitude fit provides the relevant information to tackle the differences between the two decays.

The branching-fraction ratio is obtained as

$$\frac{\mathcal{B}(B^0 \to K^{*0}\overline{K}^{*0})}{\mathcal{B}(B_s^0 \to K^{*0}\overline{K}^{*0})} = \frac{\varepsilon_{B_s^0}}{\varepsilon_{B^0}} \times \frac{\lambda_{B_s^0}^{f_L}}{\lambda_{B^0}^{f_L}} \times \frac{N_{B^0} \times f_{B^0}^D}{N_{B_s^0} \times f_{B_s^0}^D} \times \frac{f_s}{f_d}, \tag{8.1}$$

Decay mode	$B^0 \to (K^+\pi^-)(K^-\pi^+)$								
Parameter	f_L	$x_{f_\parallel}$	$|A_S^-|^2$	$x_{|A_S^+|^2}$	$x_{|A_{SS}|^2}$	$\delta_\parallel$	$\delta_\perp - \delta_S^+$	δ_S^-	δ_{SS}
Bias data-simulation	0.001	0.00	0.006	-0.001	0.004	0.01	-0.01	0.00	0.01
Fit method	0.007	0.01	0.011	0.009	0.001	0.00	0.01	0.00	0.02
Kinematic acceptance	0.005	0.01	0.006	0.004	0.002	0.03	0.12	0.01	0.04
Resolution	0.007	0.00	0.005	0.001	0.002	0.00	0.16	0.00	0.02
P-wave mass model	0.001	0.00	0.004	0.001	0.002	0.00	0.01	0.00	0.02
S-wave mass model	0.007	0.01	0.016	0.003	0.002	0.03	0.03	0.03	0.02
Differences data-simulation	0.004	0.00	0.002	0.001	0.001	0.01	0.01	0.01	0.01
Background subtraction	0.002	0.01	0.006	0.001	0.002	0.01	0.06	0.01	0.09
Peaking backgrounds	0.009	0.02	0.009	0.003	0.003	0.04	0.06	0.01	0.08
Total systematic unc.	0.016	0.03	0.024	0.011	0.006	0.06	0.22	0.04	0.13

Decay mode	$B_s^0 \to (K^+\pi^-)(K^-\pi^+)$								
Parameter	f_L	$x_{f_\parallel}$	$|A_S^-|^2$	$x_{|A_S^+|^2}$	$x_{|A_{SS}|^2}$	$\delta_\parallel$	$\delta_\perp - \delta_S^+$	δ_S^-	δ_{SS}
Bias data-simulation	0.004	0.003	0.007	-0.003	0.021	0.05	0.00	0.05	0.07
Fit method	0.001	0.000	0.001	0.000	0.000	0.00	0.00	0.00	0.00
Kinematic acceptance	0.011	0.006	0.011	0.021	0.009	0.05	0.07	0.05	0.05
Resolution	0.002	0.001	0.000	0.002	0.000	0.00	0.00	0.00	0.00
P-wave mass model	0.001	0.000	0.001	0.002	0.009	0.00	0.01	0.00	0.01
S-wave mass model	0.021	0.001	0.007	0.011	0.028	0.03	0.02	0.03	0.02
Differences data-simulation	0.002	0.000	0.001	0.001	0.001	0.01	0.00	0.01	0.01
Background subtraction	0.000	0.001	0.001	0.001	0.004	0.01	0.01	0.01	0.01
Peaking backgrounds	0.003	0.008	0.002	0.002	0.002	0.02	0.01	0.02	0.01
Time acceptance	0.008	0.014	0.008	0.004	0.005	0.00	0.00	0.00	0.00
Total systematic unc.	0.025	0.010	0.014	0.024	0.031	0.06	0.07	0.06	0.05

Table 6. Systematic uncertainties for the parameters of the amplitude-analysis fit of the $B^0_{(s)} \to (K^+\pi^-)(K^-\pi^+)$ decay. The bias related to differences between data and simulation is included in the results shown in table 4.

where, for each channel, $\varepsilon_{B^0_{(s)}}$ is the detection efficiency, $\lambda^{f_L}_{B^0_{(s)}}$ is a polarisation-dependent correction of the efficiency, originated in differences between the measured polarisation and that assumed in simulation, $N_{B^0_{(s)}}$ is the measured number of $B^0_{(s)} \to (K^+\pi^-)(K^-\pi^+)$ candidates and $f^D_{B^0_{(s)}}$ represents the VV signal purity at detection. In this way $N_{B^0_{(s)}} \times f^D_{B^0_{(s)}}$ represents the $B^0_{(s)} \to K^{*0}\overline{K}^{*0}$ yield. Finally, f_d and f_s are the hadronisation fractions of a b-quark into a B^0 and B^0_s meson, respectively.

The purity at detection and the λ^{f_L} factor ratios, $\kappa^k_{B^0_{(s)}}$, are obtained for each decay mode as

$$\kappa^k_{B^0_{(s)}} \equiv \frac{\lambda^{f_L}_{B^0_{(s)}}}{f^D_{B^0_{(s)}}} = \frac{\sum\limits_{i=1}^{6}\sum\limits_{j\geq i}^{6} \mathcal{R}e[A_i A_j^* \left(\frac{1-\eta_i}{\Gamma_H} + \frac{1+\eta_i}{\Gamma_L}\right)\omega^k_{ij}]}{(1 - |A_S^-|^2 - |A_S^+|^2 - |A_{SS}|^2) \sum\limits_{i=1}^{3}\sum\limits_{j\geq i}^{3} \mathcal{R}e[A_i^{\rm sim} A_j^{\rm sim*} \left(\frac{1-\eta_i}{\Gamma_H} + \frac{1+\eta_i}{\Gamma_L}\right)\omega^k_{ij}]},$$

(8.2)

Decay mode	$B^0 \to (K^+\pi^-)(K^-\pi^+)$				
Observable	$f_\parallel$	$f_\perp$	$|A_S^+|^2$	$|A_{SS}|^2$	S-wave fraction
Bias data-simulation	0.001	-0.001	-0.001	0.002	0.007
Fit method	0.000	0.007	0.005	0.000	0.006
Kinematic acceptance	0.003	0.004	0.001	0.003	0.006
Resolution	0.001	0.003	0.000	0.001	0.006
P-wave mass model	0.000	0.001	0.000	0.001	0.005
S-wave mass model	0.000	0.007	0.002	0.002	0.008
Differences data-simulation	0.001	0.003	0.000	0.001	0.002
Background subtraction	0.005	0.003	0.001	0.001	0.002
Peaking backgrounds	0.010	0.003	0.002	0.002	0.009
Total systematic unc.	0.012	0.012	0.007	0.004	0.017

Decay mode	$B_s^0 \to (K^+\pi^-)(K^-\pi^+)$				
Observable	$f_\parallel$	$f_\perp$	$|A_S^+|^2$	$|A_{SS}|^2$	S-wave fraction
Bias data-simulation	0.001	-0.005	-0.002	0.007	0.012
Fit method	0.001	0.001	0.000	0.001	0.001
Kinematic acceptance	0.005	0.009	0.010	0.004	0.004
Resolution	0.000	0.002	0.000	0.001	0.002
P-wave mass model	0.000	0.001	0.001	0.003	0.005
S-wave mass model	0.006	0.016	0.004	0.009	0.006
Differences data-simulation	0.001	0.001	0.000	0.001	0.001
Background subtraction	0.001	0.001	0.001	0.002	0.002
Peaking backgrounds	0.007	0.005	0.001	0.001	0.001
Time acceptance	0.008	0.016	0.003	0.001	0.007
Total systematic unc.	0.010	0.019	0.011	0.011	0.010

Table 7. Systematic uncertainties for the derived observables of the amplitude-analysis fit of the $B_{(s)}^0 \to (K^+\pi^-)(K^-\pi^+)$ decay. The bias related to differences between data and simulation is included in the results shown in table 4.

where the ω_{ij}^k coefficients are defined in eq. (6.1), $A_i^{\rm sim}$ are the amplitudes used to generate signal samples, and the η_i values are given in table 2. Also in this case, for the $B^0 \to K^{*0}\overline{K}^{*0}$ decay, the $\Gamma_{\rm H} = \Gamma_{\rm L}$ approximation is adopted.

The detection efficiency is determined from simulation for each channel separately for the different categories discussed in section 6: year of data taking, trigger type and, in addition, the LHCb magnet polarity. An exception is applied to the particle-identification selection whose efficiency is determined from large control samples of $D^{*+} \to D^0\pi^+$, $D^0 \to K^-\pi^+$ decays. Differences in kinematics and detector occupancy between the control samples and the signal data are accounted for in this particle-identification efficiency study [42, 43].

The different sources of systematic uncertainty in the branching fraction determination are discussed below.

Systematic uncertainties in the factor κ. The uncertainties on the parameters of the amplitude analysis fit described in section 7 affect the determination of the factors κ defined in eq. (8.2) as summarised in table 8.

Decay mode	$B^0 \to (K^+\pi^-)(K^-\pi^+)$				$B_s^0 \to (K^+\pi^-)(K^-\pi^+)$			
Year	2011		2012		2011		2012	
Trigger	TOS	noTOS	TOS	noTOS	TOS	noTOS	TOS	noTOS
Bias data-simulation	0.01	0.03	0.02	0.01	0.04	0.03	0.02	0.02
Fit method	0.00	0.00	0.00	0.00	0.00	0.00	0.00	0.00
Kinematic acceptance	0.03	0.04	0.02	0.02	0.06	0.06	0.06	0.06
Resolution	0.02	0.02	0.02	0.02	0.00	0.00	0.00	0.00
P-wave mass model	0.02	0.02	0.02	0.02	0.05	0.04	0.05	0.04
S-wave mass model	0.03	0.03	0.03	0.03	0.17	0.17	0.16	0.17
Differences data-simulation	0.01	0.01	0.01	0.01	0.01	0.01	0.01	0.01
Background subtraction	0.03	0.03	0.03	0.03	0.02	0.01	0.02	0.01
Peaking backgrounds	0.03	0.04	0.03	0.04	0.01	0.01	0.01	0.01
Time acceptance	–	–	–	–	0.08	0.07	0.08	0.07
Total systematic unc.	0.06	0.08	0.06	0.07	0.19	0.19	0.17	0.18

Table 8. Systematic uncertainties in the factor κ defined in eq. (8.2) split in categories. The bias originated in differences between data and simulation is corrected for in the κ results shown in table 9.

Systematic uncertainties in the signal yields. As discussed in section 7 uncertainties on the signal yields arise from the model used to fit the four-body invariant mass. The uncertainties from the different proposed alternative signal and background lineshapes are summed in quadrature to compute the final systematic uncertainty.

Systematic uncertainty in the efficiencies. A dedicated data method is employed to estimate the uncertainty in the signal efficiency originated in the PID selection.

The inputs employed for measuring the relative branching fraction are summarised in table 9. The factor κ is different for the two decay modes because of two main reasons: firstly, the discrepancy between the polarisation assumed in simulation and its measurement is larger for the $B_s^0 \to K^{*0}\overline{K}^{*0}$ than for the $B^0 \to K^{*0}\overline{K}^{*0}$ decay. Secondly, the different S-wave fraction of the decays. Also, the efficiency ratio of the two modes deviating from one is explained upon the different polarisation of the simulation samples. The LHCb detector is less efficient for values of $\cos\theta_1$ ($\cos\theta_2$) close to unity because of slow pions emitted in K^{*0} ($\overline{K}^{*0}$) decays and these are more frequent the larger is the longitudinal polarisation.

The final result of the branching-fraction ratio is obtained as the weighted mean of the per-category result obtained with eq. (8.1) for the eight categories of table 9, and found to be

$$\frac{\mathcal{B}(B^0 \to K^{*0}\overline{K}^{*0})}{\mathcal{B}(B_s^0 \to K^{*0}\overline{K}^{*0})} = 0.0758 \pm 0.0057\,(\text{stat}) \pm 0.0025\,(\text{syst}) \pm 0.0016\,\left(\frac{f_s}{f_d}\right). \qquad (8.3)$$

Considering that

$$\mathcal{B}(B_s^0 \to K^{*0}\overline{K}^{*0}) = (1.11 \pm 0.22\,(\text{stat}) \pm 0.12\,(\text{syst})) \times 10^{-5},$$

Parameter	2011 TOS *MagUp*	2011 TOS *MagDown*	2011 noTOS *MagUp*	2011 noTOS *MagDown*
N_{B^0}	$21.8 \pm\ 4.8 \pm 1.2$	$33.7 \pm\ 5.5 \pm 1.4$	$10.8 \pm\ 3.6 \pm 0.9$	$33.5 \pm\ 5.4 \pm 1.4$
$N_{B^0_s}$	$145.0 \pm 10.9 \pm 3.3$	$177.3 \pm 11.6 \pm 3.5$	$131.9 \pm 10.5 \pm 3.2$	$162.5 \pm 11.3 \pm 3.4$
$\varepsilon_{B^0_s}/\varepsilon_{B^0}$	$1.127 \pm 0.018 \pm 0.022$	$1.074 \pm 0.017 \pm 0.030$	$1.102 \pm 0.029 \pm 0.029$	$1.144 \pm 0.030 \pm 0.026$
κ_{B^0}	$1.88 \pm 0.17 \pm 0.06$		$2.11 \pm 0.21 \pm 0.08$	
$\kappa_{B^0_s}$	$3.25 \pm 0.16 \pm 0.19$		$3.27 \pm 0.16 \pm 0.19$	

Parameter	2012 TOS *MagUp*	2012 TOS *MagDown*	2012 noTOS *MagUp*	2012 noTOS *MagDown*
N_{B^0}	$73.0 \pm 8.7 \pm 2.3$	$58.7 \pm 8.1 \pm 2.1$	$64.1 \pm 8.4 \pm 2.2$	$53.7 \pm 7.9 \pm 2.1$
$N_{B^0_s}$	$311\ \pm 16\ \pm 5$	$344\ \pm 17\ \pm 5$	$346\ \pm 17\ \pm 5$	$336\ \pm 17\ \pm 5$
$\varepsilon_{B^0_s}/\varepsilon_{B^0}$	$1.102 \pm 0.014 \pm 0.053$	$1.100 \pm 0.014 \pm 0.048$	$1.180 \pm 0.022 \pm 0.065$	$1.108 \pm 0.021 \pm 0.060$
κ_{B^0}	$1.92 \pm 0.18 \pm 0.06$		$2.07 \pm 0.21 \pm 0.07$	
$\kappa_{B^0_s}$	$3.27 \pm 0.16 \pm 0.17$		$3.14 \pm 0.15 \pm 0.18$	
f_s/f_d	0.259 ± 0.015			

Table 9. Parameters used to determine $\mathcal{B}(B^0 \to K^{*0}\overline{K}^{*0})/\mathcal{B}(B^0_s \to K^{*0}\overline{K}^{*0})$. When two uncertainties are quoted, the first is statistical and the second systematic. The value of f_s/f_d is taken from ref. [44].

from ref. [5], the absolute branching fraction for the $B^0 \to K^{*0}\overline{K}^{*0}$ mode is found to be

$$\mathcal{B}(B^0 \to K^{*0}\overline{K}^{*0}) = (8.0 \pm 0.9\,(\text{stat}) \pm 0.4\,(\text{syst})) \times 10^{-7}.$$

It is worth noticing that, since the $B^0_s \to K^{*0}\overline{K}^{*0}$ branching fraction was determined with the $B^0 \to K^{*0}\phi$ decay as a reference [6], the uncertainty on f_s/f_d, which appears in the ratio of eq. (8.3), does not contribute to the absolute branching fraction measurement.

9 Summary and final considerations

The first study of $B^0 \to (K^+\pi^-)(K^-\pi^+)$ decays is performed with a data set recorded by the LHCb detector, corresponding to an integrated luminosity of $3.0\,\text{fb}^{-1}$ at centre-of-mass energies of 7 and 8 TeV. The $B^0 \to K^{*0}\overline{K}^{*0}$ mode is observed with 10.8 standard deviations. An untagged and time-integrated amplitude analysis is performed, taking into account the three helicity angles and the $(K^+\pi^-)$ and $(K^-\pi^+)$ invariant masses in a $150\,\text{MeV}/c^2$ window around the K^{*0} and $\overline{K}^{*0}$ masses. Six contributions are included in the fit: three correspond to the $B^0 \to K^{*0}\overline{K}^{*0}$ P-wave, and three to the S-wave, along with their interferences. A large longitudinal polarisation of the $B^0 \to K^{*0}\overline{K}^{*0}$ decay, $f_L = 0.724 \pm 0.051\,(\text{stat}) \pm 0.016\,(\text{syst})$, is measured. The S-wave fraction is found to be $0.408 \pm 0.050\,(\text{stat}) \pm 0.023\,(\text{syst})$.

A parallel study of the $B^0_s \to (K^+\pi^-)(K^-\pi^+)$ mode within $150\,\text{MeV}/c^2$ of the K^{*0} mass is performed, superseding a previous LHCb analysis [6]. A small longitudinal polarisation, $f_L = 0.240 \pm 0.031\,(\text{stat}) \pm 0.025\,(\text{syst})$ and a large S-wave contribution of $0.694 \pm 0.016\,(\text{stat}) \pm 0.012\,(\text{syst})$ are measured for the $B^0_s \to K^{*0}\overline{K}^{*0}$ decay, confirming the previous LHCb results of the time-dependent analysis of the same data [7].

The ratio of branching fractions

$$\frac{\mathcal{B}(B^0 \to K^{*0}\overline{K}^{*0})}{\mathcal{B}(B_s^0 \to K^{*0}\overline{K}^{*0})} = 0.0758 \pm 0.0057\,(\text{stat}) \pm 0.0025\,(\text{syst}) \pm 0.0016\left(\frac{f_s}{f_d}\right),$$

is determined. With this ratio the $B^0 \to K^{*0}\overline{K}^{*0}$ branching fraction is found to be

$$\mathcal{B}(B^0 \to K^{*0}\overline{K}^{*0}) = (8.0 \pm 0.9\,(\text{stat}) \pm 0.4\,(\text{syst})) \times 10^{-7}.$$

This value is smaller than the measurement from the BaBar collaboration [1], due to the S-wave contribution. The measurement is compatible with the QCDF prediction of ref. [3]: $(6^{+1+5}_{-1-3}) \times 10^{-7}$.

Using the B_s^0-meson averages [20] for $y \equiv \Delta\Gamma/(2\Gamma) = 0.064 \pm 0.005$ and the mixing phase, defined in eq. (2.7), $\phi_s = -0.021 \pm 0.031$, the ratio

$$R_{sd} = \frac{\mathcal{B}(B_s^0 \to K^{*0}\overline{K}^{*0})f_L(B_s^0 \to K^{*0}\overline{K}^{*0})}{\mathcal{B}(B^0 \to K^{*0}\overline{K}^{*0})f_L(B^0 \to K^{*0}\overline{K}^{*0})} \frac{1 - y^2}{1 + y\cos\phi_s}, \tag{9.1}$$

is found to be

$$R_{sd} = 3.48 \pm 0.32\,(\text{stat}) \pm 0.19\,(\text{syst}) \pm 0.08\,(f_d/f_s) \pm 0.02\,(y, \phi_s) = 3.48 \pm 0.38.$$

This result is inconsistent with the prediction of $R_{sd} = 16.4 \pm 5.2$ [13]. Within models such as QCDF or the soft-collinear effective theory, based on the heavy-quark limit the predictions, longitudinal observables, such as the one in eq. (9.1), have reduced theoretical uncertainties as compared to parallel and perpendicular ones. The heavy-quark limit also implies the polarisation hierarchy $f_L \gg f_{\parallel,\perp}$. The measured value for R_{sd} and the f_L result of the $B_s^0 \to K^{*0}\overline{K}^{*0}$ decay put in question this hierarchy. The picture is even more intriguing since, contrary to its U-spin partner, the $B^0 \to K^{*0}\overline{K}^{*0}$ decay is confirmed to be strongly polarised.

Acknowledgments

References

[1] BaBar collaboration, *Observation of $B^0 \to K^{*0} \bar{K}^{*0}$ and search for $B^0 \to K^{*0}K^{*0}$*, *Phys. Rev. Lett.* **100** (2008) 081801 [`arXiv:0708.2248`] [InSPIRE].

[2] Belle collaboration, *Search for $B^0 \to K^{*0}\overline{K}^{*0}$, $B^0 \to K^{*0}K^{*0}$ and $B^0 \to K^+\pi^- K^\mp \pi^\pm$ decays*, *Phys. Rev.* **D 81** (2010) 071101 [`arXiv:1001.4595`] [InSPIRE].

[3] M. Beneke, J. Rohrer and D. Yang, *Branching fractions, polarisation and asymmetries of $B \to VV$ decays*, *Nucl. Phys.* **B 774** (2007) 64 [`hep-ph/0612290`] [InSPIRE].

[4] LHCb collaboration, *First observation of the decay $B_s^0 \to K^{*0}\bar{K}^{*0}$*, *Phys. Lett.* **B 709** (2012) 50 [`arXiv:1111.4183`] [InSPIRE].

[5] Particle Data Group collaboration, *Review of particle physics*, *Phys. Rev.* **D 98** (2018) 030001 [InSPIRE].

[6] LHCb collaboration, *Measurement of CP asymmetries and polarisation fractions in $B_s^0 \to K^{*0}\bar{K}^{*0}$ decays*, *JHEP* **07** (2015) 166 [`arXiv:1503.05362`] [InSPIRE].

[7] LHCb collaboration, *First measurement of the CP-violating phase $\phi_s^{d\bar{d}}$ in $B_s^0 \to (K^+\pi^-)(K^-\pi^+)$ decays*, *JHEP* **03** (2018) 140 [`arXiv:1712.08683`] [InSPIRE].

[8] A.L. Kagan, *Polarization in $B \to VV$ decays*, *Phys. Lett.* **B 601** (2004) 151 [`hep-ph/0405134`] [InSPIRE].

[9] Belle-II collaboration, *The Belle II physics book*, `arXiv:1808.10567` [InSPIRE].

[10] M. Ciuchini, M. Pierini and L. Silvestrini, *B_s to $K^{*0}\bar{K}^{*0}$ decays: the golden channels for new physics searches*, *Phys. Rev. Lett.* **100** (2008) 031802 [`hep-ph/0703137`] [InSPIRE].

[11] LHCb collaboration, *Physics case for an LHCb Upgrade II — opportunities in flavour physics and beyond, in the HL-LHC era*, `arXiv:1808.08865` [InSPIRE].

[12] S. Descotes-Genon, J. Matias and J. Virto, *Penguin-mediated $B_{d,s} \to VV$ decays and the B_s–$\bar{B}_s$ mixing angle*, *Phys. Rev.* **D 76** (2007) 074005 [*Erratum ibid.* **D 84** (2011) 039901] [`arXiv:0705.0477`] [InSPIRE].

[13] S. Descotes-Genon, J. Matias and J. Virto, *An analysis of $B_{d,s}$ mixing angles in presence of new physics and an update of $B_s \to K^{*0}\bar{K}^{*0}$*, *Phys. Rev.* **D 85** (2012) 034010 [`arXiv:1111.4882`] [InSPIRE].

[14] G.N. Fleming, *Recoupling effects in the isobar model. 1. General formalism for three-pion scattering*, *Phys. Rev.* **135** (1964) B551 [InSPIRE].

[15] D. Morgan, *Phenomenological analysis of $I = 12$ single-pion production processes in the energy range 500 to 700 MeV*, *Phys. Rev.* **166** (1968) 1731 [InSPIRE].

[16] D. Herndon, P. Soding and R.J. Cashmore, *A generalized isobar model formalism*, *Phys. Rev.* **D 11** (1975) 3165 [INSPIRE].

[17] D. Aston et al., *A study of $K^-\pi^+$ scattering in the reaction $K^-p \to K^-\pi^+n$ at 11 GeV/c*, *Nucl. Phys.* **B 296** (1988) 493 [INSPIRE].

[18] BaBar collaboration, *Time-dependent and time-integrated angular analysis of $B \to \phi K_s\pi^0$ and $B \to \phi K^+\pi^-$*, *Phys. Rev.* **D 78** (2008) 092008 [arXiv:0808.3586] [INSPIRE].

[19] B. Bhattacharya, A. Datta, M. Duraisamy and D. London, *Searching for new physics with $b^- \to s^- B_s^0 \to V_1 V_2$ penguin decays*, *Phys. Rev.* **D 88** (2013) 016007 [arXiv:1306.1911] [INSPIRE].

[20] HFLAV collaboration, *Averages of b-hadron, c-hadron and τ-lepton properties as of summer 2016*, *Eur. Phys. J.* **C 77** (2017) 895 [arXiv:1612.07233] [INSPIRE], updated results and plots available at https://hflav.web.cern.ch.

[21] LHCb collaboration, *The LHCb detector at the LHC*, 2008 *JINST* **3** S08005 [INSPIRE].

[22] LHCb collaboration, *LHCb detector performance*, *Int. J. Mod. Phys.* **A 30** (2015) 1530022 [arXiv:1412.6352] [INSPIRE].

[23] R. Aaij et al., *The LHCb Trigger and its performance in 2011*, 2013 *JINST* **8** P04022 [arXiv:1211.3055] [INSPIRE].

[24] T. Sjöstrand, S. Mrenna and P.Z. Skands, *PYTHIA 6.4 physics and manual*, *JHEP* **05** (2006) 026 [hep-ph/0603175] [INSPIRE].

[25] I. Belyaev et al., *Handling of the generation of primary events in Gauss, the LHCb simulation framework*, *IEEE Nucl. Sci. Symp. Conf. Rec. (NSS/MIC)* (2010) 1155.

[26] D.J. Lange, *The EvtGen particle decay simulation package*, *Nucl. Instrum. Meth.* **A 462** (2001) 152 [INSPIRE].

[27] P. Golonka and Z. Was, *PHOTOS Monte Carlo: a precision tool for QED corrections in Z and W decays*, *Eur. Phys. J.* **C 45** (2006) 97 [hep-ph/0506026] [INSPIRE].

[28] Geant4 collaboration, *GEANT4 developments and applications*, *IEEE Trans. Nucl. Sci.* **53** (2006) 270.

[29] Geant4 collaboration, *GEANT4: a simulation toolkit*, *Nucl. Instrum. Meth.* **A 506** (2003) 250 [INSPIRE].

[30] M. Clemencic et al., *The LHCb simulation application, gauss: design, evolution and experience*, *J. Phys. Conf. Ser.* **331** (2011) 032023 [INSPIRE].

[31] L. Breiman J.H. Friedman, R.A. Olshen and C.J. Stone, *Classification and regression trees*, Wadsworth international group, Belmont U.S.A. (1984).

[32] B.P. Roe et al., *Boosted decision trees, an alternative to artificial neural networks*, *Nucl. Instrum. Meth.* **A 543** (2005) 577 [physics/0408124] [INSPIRE].

[33] D. Martínez Santos and F. Dupertuis, *Mass distributions marginalized over per-event errors*, *Nucl. Instrum. Meth.* **A 764** (2014) 150 [arXiv:1312.5000] [INSPIRE].

[34] T. Skwarnicki, *A study of the radiative cascade transitions between the Υ' and Υ resonances*, Ph.D. thesis, Institute of Nuclear Physics, Krakow, Poland (1986) [DESY-F31-86-02].

[35] ARGUS collaboration, *Exclusive hadronic decays of B mesons*, *Z. Phys.* **C 48** (1990) 543 [INSPIRE].

[36] M. Pivk and F.R. Le Diberder, *SPlot: a statistical tool to unfold data distributions*, *Nucl. Instrum. Meth.* **A 555** (2005) 356 [physics/0402083] [INSPIRE].

[37] Y. Xie, *sFit: a method for background subtraction in maximum likelihood fit*, arXiv:0905.0724 [INSPIRE].

[38] T. du Pree, *Search for a strange phase in beautiful oscillations*, Ph.D. thesis, Vrije Universiteit Amsterdam, Amsterdam, The Netherlands (2010) [CERN-THESIS-2010-124].

[39] LHCb collaboration, *Observation of the resonant character of the $Z(4430)^-$ state*, *Phys. Rev. Lett.* **112** (2014) 222002 [arXiv:1404.1903] [INSPIRE].

[40] J.R. Pelaez and A. Rodas, *Pion-kaon scattering amplitude constrained with forward dispersion relations up to $1.6\,GeV$*, *Phys. Rev.* **D 93** (2016) 074025 [arXiv:1602.08404] [INSPIRE].

[41] J. García Pardiñas, *Search for flavour anomalies at LHCb: decay-time-dependent CP violation in $B_s^0 \to (K^+\pi^-)(K^-\pi^+)$ and lepton universality in $\overline{B}^0 \to D^{(*)+}l\overline{\nu}_l$*, Ph.D. thesis, Universidade de Santiago de Compostela, Santiago de Compostela, Spain (2018) [CERN-THESIS-2018-096].

[42] M. Adinolfi et al., *Performance of the LHCb RICH detector at the LHC*, *Eur. Phys. J.* **C 73** (2013) 2431 [arXiv:1211.6759] [INSPIRE].

[43] L. Anderlini et al., *The PIDCalib package*, LHCb-PUB-2016-021 (2016).

[44] LHCb collaboration, *Updated average f_s/f_d b-hadron production fraction ratio for $7\,TeV\,pp$ collisions*, LHCb-CONF-2013-011 (2013).

The LHCb collaboration

R. Aaij[29], C. Abellán Beteta[46], B. Adeva[43], M. Adinolfi[50], C.A. Aidala[77], Z. Ajaltouni[7],
S. Akar[61], P. Albicocco[20], J. Albrecht[12], F. Alessio[44], M. Alexander[55], A. Alfonso Albero[42],
G. Alkhazov[35], P. Alvarez Cartelle[57], A.A. Alves Jr[43], S. Amato[2], Y. Amhis[9], L. An[19],
L. Anderlini[19], G. Andreassi[45], M. Andreotti[18], J.E. Andrews[62], F. Archilli[29], J. Arnau Romeu[8],
A. Artamonov[41], M. Artuso[63], K. Arzymatov[39], E. Aslanides[8], M. Atzeni[46], B. Audurier[24],
S. Bachmann[14], J.J. Back[52], S. Baker[57], V. Balagura[9,b], W. Baldini[18,44], A. Baranov[39],
R.J. Barlow[58], S. Barsuk[9], W. Barter[57], M. Bartolini[21], F. Baryshnikov[73], V. Batozskaya[33],
B. Batsukh[63], A. Battig[12], V. Battista[45], A. Bay[45], F. Bedeschi[26], I. Bediaga[1], A. Beiter[63],
L.J. Bel[29], S. Belin[24], N. Beliy[4], V. Bellee[45], N. Belloli[22,i], K. Belous[41], I. Belyaev[36],
G. Bencivenni[20], E. Ben-Haim[10], S. Benson[29], S. Beranek[11], A. Berezhnoy[37], R. Bernet[46],
D. Berninghoff[14], E. Bertholet[10], A. Bertolin[25], C. Betancourt[46], F. Betti[17,e], M.O. Bettler[51],
Ia. Bezshyiko[46], S. Bhasin[50], J. Bhom[31], M.S. Bieker[12], S. Bifani[49], P. Billoir[10], A. Birnkraut[12],
A. Bizzeti[19,u], M. Bjørn[59], M.P. Blago[44], T. Blake[52], F. Blanc[45], S. Blusk[63], D. Bobulska[55],
V. Bocci[28], O. Boente Garcia[43], T. Boettcher[60], A. Bondar[40,x], N. Bondar[35], S. Borghi[58,44],
M. Borisyak[39], M. Borsato[14], M. Boubdir[11], T.J.V. Bowcock[56], C. Bozzi[18,44], S. Braun[14],
M. Brodski[44], J. Brodzicka[31], A. Brossa Gonzalo[52], D. Brundu[24,44], E. Buchanan[50],
A. Buonaura[46], C. Burr[58], A. Bursche[24], J. Buytaert[44], W. Byczynski[44], S. Cadeddu[24], H. Cai[67],
R. Calabrese[18,g], R. Calladine[49], M. Calvi[22,i], M. Calvo Gomez[42,m], A. Camboni[42,m],
P. Campana[20], D.H. Campora Perez[44], L. Capriotti[17,e], A. Carbone[17,e], G. Carboni[27],
R. Cardinale[21], A. Cardini[24], P. Carniti[22,i], K. Carvalho Akiba[2], G. Casse[56], M. Cattaneo[44],
G. Cavallero[21], R. Cenci[26,p], M.G. Chapman[50], M. Charles[10,44], Ph. Charpentier[44],
G. Chatzikonstantinidis[49], M. Chefdeville[6], V. Chekalina[39], C. Chen[3], S. Chen[24], S.-G. Chitic[44],
V. Chobanova[43], M. Chrzaszcz[44], A. Chubykin[35], P. Ciambrone[20], X. Cid Vidal[43], G. Ciezarek[44],
F. Cindolo[17], P.E.L. Clarke[54], M. Clemencic[44], H.V. Cliff[51], J. Closier[44], V. Coco[44],
J.A.B. Coelho[9], J. Cogan[8], E. Cogneras[7], L. Cojocariu[34], P. Collins[44], T. Colombo[44],
A. Comerma-Montells[14], A. Contu[24], G. Coombs[44], S. Coquereau[42], G. Corti[44],
C.M. Costa Sobral[52], B. Couturier[44], G.A. Cowan[54], D.C. Craik[60], A. Crocombe[52],
M. Cruz Torres[1], R. Currie[54], C.L. Da Silva[78], E. Dall'Occo[29], J. Dalseno[43,v], C. D'Ambrosio[44],
A. Danilina[36], P. d'Argent[14], A. Davis[58], O. De Aguiar Francisco[44], K. De Bruyn[44],
S. De Capua[58], M. De Cian[45], J.M. De Miranda[1], L. De Paula[2], M. De Serio[16,d], P. De Simone[20],
J.A. de Vries[29], C.T. Dean[55], W. Dean[77], D. Decamp[6], L. Del Buono[10], B. Delaney[51],
H.-P. Dembinski[13], M. Demmer[12], A. Dendek[32], D. Derkach[74], O. Deschamps[7], F. Desse[9],
F. Dettori[24], B. Dey[68], A. Di Canto[44], P. Di Nezza[20], S. Didenko[73], H. Dijkstra[44], F. Dordei[24],
M. Dorigo[44,y], A.C. dos Reis[1], A. Dosil Suárez[43], L. Douglas[55], A. Dovbnya[47], K. Dreimanis[56],
L. Dufour[44], G. Dujany[10], P. Durante[44], J.M. Durham[78], D. Dutta[58], R. Dzhelyadin[41,†],
M. Dziewiecki[14], A. Dziurda[31], A. Dzyuba[35], S. Easo[53], U. Egede[57], V. Egorychev[36],
S. Eidelman[40,x], S. Eisenhardt[54], U. Eitschberger[12], R. Ekelhof[12], L. Eklund[55], S. Ely[63],
A. Ene[34], S. Escher[11], S. Esen[29], T. Evans[61], A. Falabella[17], C. Färber[44], N. Farley[49], S. Farry[56],
D. Fazzini[22,i], M. Féo[44], P. Fernandez Declara[44], A. Fernandez Prieto[43], F. Ferrari[17,e],
L. Ferreira Lopes[45], F. Ferreira Rodrigues[2], S. Ferreres Sole[29], M. Ferro-Luzzi[44], S. Filippov[38],
R.A. Fini[16], M. Fiorini[18,g], M. Firlej[32], C. Fitzpatrick[45], T. Fiutowski[32], F. Fleuret[9,b],
M. Fontana[44], F. Fontanelli[21,h], R. Forty[44], V. Franco Lima[56], M. Frank[44], C. Frei[44], J. Fu[23,q],
W. Funk[44], E. Gabriel[54], A. Gallas Torreira[43], D. Galli[17,e], S. Gallorini[25], S. Gambetta[54],
Y. Gan[3], M. Gandelman[2], P. Gandini[23], Y. Gao[3], L.M. Garcia Martin[76], J. García Pardiñas[46],
B. Garcia Plana[43], J. Garra Tico[51], L. Garrido[42], D. Gascon[42], C. Gaspar[44], G. Gazzoni[7],
D. Gerick[14], E. Gersabeck[58], M. Gersabeck[58], T. Gershon[52], D. Gerstel[8], Ph. Ghez[6], V. Gibson[51],

– 25 –

O.G. Girard[45], P. Gironella Gironell[42], L. Giubega[34], K. Gizdov[54], V.V. Gligorov[10], C. Göbel[65],
D. Golubkov[36], A. Golutvin[57,73], A. Gomes[1,a], I.V. Gorelov[37], C. Gotti[22,i], E. Govorkova[29],
J.P. Grabowski[14], R. Graciani Diaz[42], L.A. Granado Cardoso[44], E. Graugés[42], E. Graverini[46],
G. Graziani[19], A. Grecu[34], R. Greim[29], P. Griffith[24], L. Grillo[58], L. Gruber[44],
B.R. Gruberg Cazon[59], C. Gu[3], E. Gushchin[38], A. Guth[11], Yu. Guz[41,44], T. Gys[44],
T. Hadavizadeh[59], C. Hadjivasiliou[7], G. Haefeli[45], C. Haen[44], S.C. Haines[51], B. Hamilton[62],
X. Han[14], T.H. Hancock[59], S. Hansmann-Menzemer[14], N. Harnew[59], T. Harrison[56], C. Hasse[44],
M. Hatch[44], J. He[4], M. Hecker[57], K. Heinicke[12], A. Heister[12], K. Hennessy[56], L. Henry[76],
M. Heß[70], J. Heuel[11], A. Hicheur[64], R. Hidalgo Charman[58], D. Hill[59], M. Hilton[58],
P.H. Hopchev[45], J. Hu[14], W. Hu[68], W. Huang[4], Z.C. Huard[61], W. Hulsbergen[29], T. Humair[57],
M. Hushchyn[74], D. Hutchcroft[56], D. Hynds[29], P. Ibis[12], M. Idzik[32], P. Ilten[49], A. Inglessi[35],
A. Inyakin[41], K. Ivshin[35], R. Jacobsson[44], S. Jakobsen[44], J. Jalocha[59], E. Jans[29], B.K. Jashal[76],
A. Jawahery[62], F. Jiang[3], M. John[59], D. Johnson[44], C.R. Jones[51], C. Joram[44], B. Jost[44],
N. Jurik[59], S. Kandybei[47], M. Karacson[44], J.M. Kariuki[50], S. Karodia[55], N. Kazeev[74],
M. Kecke[14], F. Keizer[51], M. Kelsey[63], M. Kenzie[51], T. Ketel[30], B. Khanji[44], A. Kharisova[75],
C. Khurewathanakul[45], K.E. Kim[63], T. Kirn[11], V.S. Kirsebom[45], S. Klaver[20], K. Klimaszewski[33],
S. Koliiev[48], M. Kolpin[14], R. Kopecna[14], P. Koppenburg[29], I. Kostiuk[29,48], S. Kotriakhova[35],
M. Kozeiha[7], L. Kravchuk[38], M. Kreps[52], F. Kress[57], S. Kretzschmar[11], P. Krokovny[40,x],
W. Krupa[32], W. Krzemien[33], W. Kucewicz[31,l], M. Kucharczyk[31], V. Kudryavtsev[40,x],
G.J. Kunde[78], A.K. Kuonen[45], T. Kvaratskheliya[36], D. Lacarrere[44], G. Lafferty[58], A. Lai[24],
D. Lancierini[46], G. Lanfranchi[20], C. Langenbruch[11], T. Latham[52], C. Lazzeroni[49], R. Le Gac[8],
R. Lefèvre[7], A. Leflat[37], F. Lemaitre[44], O. Leroy[8], T. Lesiak[31], B. Leverington[14], H. Li[66],
P.-R. Li[4,ab], X. Li[78], Y. Li[5], Z. Li[63], X. Liang[63], T. Likhomanenko[72], R. Lindner[44], F. Lionetto[46],
V. Lisovskyi[9], G. Liu[66], X. Liu[3], D. Loh[52], A. Loi[24], I. Longstaff[55], J.H. Lopes[2], G. Loustau[46],
G.H. Lovell[51], D. Lucchesi[25,o], M. Lucio Martinez[43], Y. Luo[3], A. Lupato[25], E. Luppi[18,g],
O. Lupton[52], A. Lusiani[26], X. Lyu[4], F. Machefert[9], F. Maciuc[34], V. Macko[45], P. Mackowiak[12],
S. Maddrell-Mander[50], O. Maev[35,44], K. Maguire[58], D. Maisuzenko[35], M.W. Majewski[32],
S. Malde[59], B. Malecki[44], A. Malinin[72], T. Maltsev[40,x], H. Malygina[14], G. Manca[24,f],
G. Mancinelli[8], D. Marangotto[23,q], J. Maratas[7,w], J.F. Marchand[6], U. Marconi[17],
C. Marin Benito[9], M. Marinangeli[45], P. Marino[45], J. Marks[14], P.J. Marshall[56], G. Martellotti[28],
M. Martinelli[44,22,i], D. Martinez Santos[43], F. Martinez Vidal[76], A. Massafferri[1], M. Materok[11],
R. Matev[44], A. Mathad[46], Z. Mathe[44], V. Matiunin[36], C. Matteuzzi[22], K.R. Mattioli[77],
A. Mauri[46], E. Maurice[9,b], B. Maurin[45], M. McCann[57,44], A. McNab[58], R. McNulty[15],
J.V. Mead[56], B. Meadows[61], C. Meaux[8], N. Meinert[70], D. Melnychuk[33], M. Merk[29], A. Merli[23,q],
E. Michielin[25], D.A. Milanes[69], E. Millard[52], M.-N. Minard[6], O. Mineev[36], L. Minzoni[18,g],
D.S. Mitzel[14], A. Mödden[12], A. Mogini[10], R.D. Moise[57], T. Mombächer[12], I.A. Monroy[69],
S. Monteil[7], M. Morandin[25], G. Morello[20], M.J. Morello[26,t], J. Moron[32], A.B. Morris[8],
R. Mountain[63], F. Muheim[54], M. Mukherjee[68], M. Mulder[29], D. Müller[44], J. Müller[12],
K. Müller[46], V. Müller[12], C.H. Murphy[59], D. Murray[58], P. Naik[50], T. Nakada[45],
R. Nandakumar[53], A. Nandi[59], T. Nanut[45], I. Nasteva[2], M. Needham[54], N. Neri[23,q], S. Neubert[14],
N. Neufeld[44], R. Newcombe[57], T.D. Nguyen[45], C. Nguyen-Mau[45,n], S. Nieswand[11], R. Niet[12],
N. Nikitin[37], N.S. Nolte[44], A. Oblakowska-Mucha[32], V. Obraztsov[41], S. Ogilvy[55],
D.P. O'Hanlon[17], R. Oldeman[24,f], C.J.G. Onderwater[71], J. D. Osborn[77], A. Ossowska[31],
J.M. Otalora Goicochea[2], T. Ovsiannikova[36], P. Owen[46], A. Oyanguren[76], P.R. Pais[45],
T. Pajero[26,t], A. Palano[16], M. Palutan[20], G. Panshin[75], A. Papanestis[53], M. Pappagallo[54],
L.L. Pappalardo[18,g], W. Parker[62], C. Parkes[58,44], G. Passaleva[19,44], A. Pastore[16], M. Patel[57],
C. Patrignani[17,e], A. Pearce[44], A. Pellegrino[29], G. Penso[28], M. Pepe Altarelli[44], S. Perazzini[44],
D. Pereima[36], P. Perret[7], L. Pescatore[45], K. Petridis[50], A. Petrolini[21,h], A. Petrov[72],

S. Petrucci[54], M. Petruzzo[23,q], B. Pietrzyk[6], G. Pietrzyk[45], M. Pikies[31], M. Pili[59], D. Pinci[28],
J. Pinzino[44], F. Pisani[44], A. Piucci[14], V. Placinta[34], S. Playfer[54], J. Plews[49], M. Plo Casasus[43],
F. Polci[10], M. Poli Lener[20], M. Poliakova[63], A. Poluektov[8], N. Polukhina[73,c], I. Polyakov[63],
E. Polycarpo[2], G.J. Pomery[50], S. Ponce[44], A. Popov[41], D. Popov[49,13], S. Poslavskii[41], E. Price[50],
C. Prouve[43], V. Pugatch[48], A. Puig Navarro[46], H. Pullen[59], G. Punzi[26,p], W. Qian[4], J. Qin[4],
R. Quagliani[10], B. Quintana[7], N.V. Raab[15], B. Rachwal[32], J.H. Rademacker[50], M. Rama[26],
M. Ramos Pernas[43], M.S. Rangel[2], F. Ratnikov[39,74], G. Raven[30], M. Ravonel Salzgeber[44],
M. Reboud[6], F. Redi[45], S. Reichert[12], F. Reiss[10], C. Remon Alepuz[76], Z. Ren[3], V. Renaudin[59],
S. Ricciardi[53], S. Richards[50], K. Rinnert[56], P. Robbe[9], A. Robert[10], A.B. Rodrigues[45],
E. Rodrigues[61], J.A. Rodriguez Lopez[69], M. Roehrken[44], S. Roiser[44], A. Rollings[59],
V. Romanovskiy[41], A. Romero Vidal[43], J.D. Roth[77], M. Rotondo[20], M.S. Rudolph[63], T. Ruf[44],
J. Ruiz Vidal[76], J.J. Saborido Silva[43], N. Sagidova[35], B. Saitta[24,f], V. Salustino Guimaraes[65],
C. Sanchez Gras[29], C. Sanchez Mayordomo[76], B. Sanmartin Sedes[43], R. Santacesaria[28],
C. Santamarina Rios[43], M. Santimaria[20,44], E. Santovetti[27,j], G. Sarpis[58], A. Sarti[20,k],
C. Satriano[28,s], A. Satta[27], M. Saur[4], D. Savrina[36,37], S. Schael[11], M. Schellenberg[12],
M. Schiller[55], H. Schindler[44], M. Schmelling[13], T. Schmelzer[12], B. Schmidt[44], O. Schneider[45],
A. Schopper[44], H.F. Schreiner[61], M. Schubiger[45], S. Schulte[45], M.H. Schune[9], R. Schwemmer[44],
B. Sciascia[20], A. Sciubba[28,k], A. Semennikov[36], E.S. Sepulveda[10], A. Sergi[49,44], N. Serra[46],
J. Serrano[8], L. Sestini[25], A. Seuthe[12], P. Seyfert[44], M. Shapkin[41], T. Shears[56], L. Shekhtman[40,x],
V. Shevchenko[72], E. Shmanin[73], B.G. Siddi[18], R. Silva Coutinho[46], L. Silva de Oliveira[2],
G. Simi[25,o], S. Simone[16,d], I. Skiba[18], N. Skidmore[14], T. Skwarnicki[63], M.W. Slater[49],
J.G. Smeaton[51], E. Smith[11], I.T. Smith[54], M. Smith[57], M. Soares[17], l. Soares Lavra[1],
M.D. Sokoloff[61], F.J.P. Soler[55], B. Souza De Paula[2], B. Spaan[12], E. Spadaro Norella[23,q],
P. Spradlin[55], F. Stagni[44], M. Stahl[14], S. Stahl[44], P. Stefko[45], S. Stefkova[57], O. Steinkamp[46],
S. Stemmle[14], O. Stenyakin[41], M. Stepanova[35], H. Stevens[12], A. Stocchi[9], S. Stone[63], S. Stracka[26],
M.E. Stramaglia[45], M. Straticiuc[34], U. Straumann[46], S. Strokov[75], J. Sun[3], L. Sun[67], Y. Sun[62],
K. Swientek[32], A. Szabelski[33], T. Szumlak[32], M. Szymanski[4], Z. Tang[3], T. Tekampe[12],
G. Tellarini[18], F. Teubert[44], E. Thomas[44], M.J. Tilley[57], V. Tisserand[7], S. T'Jampens[6],
M. Tobin[5], S. Tolk[44], L. Tomassetti[18,g], D. Tonelli[26], D.Y. Tou[10], R. Tourinho Jadallah Aoude[1],
E. Tournefier[6], M. Traill[55], M.T. Tran[45], A. Trisovic[51], A. Tsaregorodtsev[8], G. Tuci[26,44,p],
A. Tully[51], N. Tuning[29], A. Ukleja[33], A. Usachov[9], A. Ustyuzhanin[39,74], U. Uwer[14], A. Vagner[75],
V. Vagnoni[17], A. Valassi[44], S. Valat[44], G. Valenti[17], M. van Beuzekom[29], H. Van Hecke[78],
E. van Herwijnen[44], C.B. Van Hulse[15], J. van Tilburg[29], M. van Veghel[29], R. Vazquez Gomez[44],
P. Vazquez Regueiro[43], C. Vázquez Sierra[29], S. Vecchi[18], J.J. Velthuis[50], M. Veltri[19,r],
A. Venkateswaran[63], M. Vernet[7], M. Veronesi[29], M. Vesterinen[52], J.V. Viana Barbosa[44],
D. Vieira[4], M. Vieites Diaz[43], H. Viemann[70], X. Vilasis-Cardona[42,m], A. Vitkovskiy[29], M. Vitti[51],
V. Volkov[37], A. Vollhardt[46], D. Vom Bruch[10], B. Voneki[44], A. Vorobyev[35], V. Vorobyev[40,x],
N. Voropaev[35], R. Waldi[70], J. Walsh[26], J. Wang[5], M. Wang[3], Y. Wang[68], Z. Wang[46],
D.R. Ward[51], H.M. Wark[56], N.K. Watson[49], D. Websdale[57], A. Weiden[46], C. Weisser[60],
M. Whitehead[11], G. Wilkinson[59], M. Wilkinson[63], I. Williams[51], M. Williams[60],
M.R.J. Williams[58], T. Williams[49], F.F. Wilson[53], M. Winn[9], W. Wislicki[33], M. Witek[31],
G. Wormser[9], S.A. Wotton[51], K. Wyllie[44], D. Xiao[68], Y. Xie[68], H. Xing[66], A. Xu[3], M. Xu[68],
Q. Xu[4], Z. Xu[6], Z. Xu[3], Z. Yang[3], Z. Yang[62], Y. Yao[63], L.E. Yeomans[56], H. Yin[68], J. Yu[68,aa],
X. Yuan[63], O. Yushchenko[41], K.A. Zarebski[49], M. Zavertyaev[13,c], M. Zeng[3], D. Zhang[68],
L. Zhang[3], W.C. Zhang[3,z], Y. Zhang[44], A. Zhelezov[14], Y. Zheng[4], X. Zhu[3], V. Zhukov[11,37],
J.B. Zonneveld[54], S. Zucchelli[17,e]

1   *Centro Brasileiro de Pesquisas Físicas (CBPF), Rio de Janeiro, Brazil*
2   *Universidade Federal do Rio de Janeiro (UFRJ), Rio de Janeiro, Brazil*

[3] *Center for High Energy Physics, Tsinghua University, Beijing, China*

[4] *University of Chinese Academy of Sciences, Beijing, China*

[5] *Institute Of High Energy Physics (ihep), Beijing, China*

[6] *Univ. Grenoble Alpes, Univ. Savoie Mont Blanc, CNRS, IN2P3-LAPP, Annecy, France*

[7] *Université Clermont Auvergne, CNRS/IN2P3, LPC, Clermont-Ferrand, France*

[8] *Aix Marseille Univ, CNRS/IN2P3, CPPM, Marseille, France*

[9] *LAL, Univ. Paris-Sud, CNRS/IN2P3, Université Paris-Saclay, Orsay, France*

[10] *LPNHE, Sorbonne Université, Paris Diderot Sorbonne Paris Cité, CNRS/IN2P3, Paris, France*

[11] *I. Physikalisches Institut, RWTH Aachen University, Aachen, Germany*

[12] *Fakultät Physik, Technische Universität Dortmund, Dortmund, Germany*

[13] *Max-Planck-Institut für Kernphysik (MPIK), Heidelberg, Germany*

[14] *Physikalisches Institut, Ruprecht-Karls-Universität Heidelberg, Heidelberg, Germany*

[15] *School of Physics, University College Dublin, Dublin, Ireland*

[16] *INFN Sezione di Bari, Bari, Italy*

[17] *INFN Sezione di Bologna, Bologna, Italy*

[18] *INFN Sezione di Ferrara, Ferrara, Italy*

[19] *INFN Sezione di Firenze, Firenze, Italy*

[20] *INFN Laboratori Nazionali di Frascati, Frascati, Italy*

[21] *INFN Sezione di Genova, Genova, Italy*

[22] *INFN Sezione di Milano-Bicocca, Milano, Italy*

[23] *INFN Sezione di Milano, Milano, Italy*

[24] *INFN Sezione di Cagliari, Monserrato, Italy*

[25] *INFN Sezione di Padova, Padova, Italy*

[26] *INFN Sezione di Pisa, Pisa, Italy*

[27] *INFN Sezione di Roma Tor Vergata, Roma, Italy*

[28] *INFN Sezione di Roma La Sapienza, Roma, Italy*

[29] *Nikhef National Institute for Subatomic Physics, Amsterdam, Netherlands*

[30] *Nikhef National Institute for Subatomic Physics and VU University Amsterdam, Amsterdam, Netherlands*

[31] *Henryk Niewodniczanski Institute of Nuclear Physics Polish Academy of Sciences, Kraków, Poland*

[32] *AGH — University of Science and Technology, Faculty of Physics and Applied Computer Science, Kraków, Poland*

[33] *National Center for Nuclear Research (NCBJ), Warsaw, Poland*

[34] *Horia Hulubei National Institute of Physics and Nuclear Engineering, Bucharest-Magurele, Romania*

[35] *Petersburg Nuclear Physics Institute NRC Kurchatov Institute (PNPI NRC KI), Gatchina, Russia*

[36] *Institute of Theoretical and Experimental Physics NRC Kurchatov Institute (ITEP NRC KI), Moscow, Russia, Moscow, Russia*

[37] *Institute of Nuclear Physics, Moscow State University (SINP MSU), Moscow, Russia*

[38] *Institute for Nuclear Research of the Russian Academy of Sciences (INR RAS), Moscow, Russia*

[39] *Yandex School of Data Analysis, Moscow, Russia*

[40] *Budker Institute of Nuclear Physics (SB RAS), Novosibirsk, Russia*

[41] *Institute for High Energy Physics NRC Kurchatov Institute (IHEP NRC KI), Protvino, Russia, Protvino, Russia*

[42] *ICCUB, Universitat de Barcelona, Barcelona, Spain*

[43] *Instituto Galego de Física de Altas Enerxías (IGFAE), Universidade de Santiago de Compostela, Santiago de Compostela, Spain*

[44] *European Organization for Nuclear Research (CERN), Geneva, Switzerland*

[45] *Institute of Physics, Ecole Polytechnique Fédérale de Lausanne (EPFL), Lausanne, Switzerland*

[46] *Physik-Institut, Universität Zürich, Zürich, Switzerland*

[47] *NSC Kharkiv Institute of Physics and Technology (NSC KIPT), Kharkiv, Ukraine*

[48] *Institute for Nuclear Research of the National Academy of Sciences (KINR), Kyiv, Ukraine*

[49] University of Birmingham, Birmingham, United Kingdom
[50] H.H. Wills Physics Laboratory, University of Bristol, Bristol, United Kingdom
[51] Cavendish Laboratory, University of Cambridge, Cambridge, United Kingdom
[52] Department of Physics, University of Warwick, Coventry, United Kingdom
[53] STFC Rutherford Appleton Laboratory, Didcot, United Kingdom
[54] School of Physics and Astronomy, University of Edinburgh, Edinburgh, United Kingdom
[55] School of Physics and Astronomy, University of Glasgow, Glasgow, United Kingdom
[56] Oliver Lodge Laboratory, University of Liverpool, Liverpool, United Kingdom
[57] Imperial College London, London, United Kingdom
[58] School of Physics and Astronomy, University of Manchester, Manchester, United Kingdom
[59] Department of Physics, University of Oxford, Oxford, United Kingdom
[60] Massachusetts Institute of Technology, Cambridge, MA, U.S.A.
[61] University of Cincinnati, Cincinnati, OH, U.S.A.
[62] University of Maryland, College Park, MD, U.S.A.
[63] Syracuse University, Syracuse, NY, U.S.A.
[64] Laboratory of Mathematical and Subatomic Physics , Constantine, Algeria, associated to[2]
[65] Pontifícia Universidade Católica do Rio de Janeiro (PUC-Rio), Rio de Janeiro, Brazil, associated to[2]
[66] South China Normal University, Guangzhou, China, associated to[3]
[67] School of Physics and Technology, Wuhan University, Wuhan, China, associated to[3]
[68] Institute of Particle Physics, Central China Normal University, Wuhan, Hubei, China, associated to[3]
[69] Departamento de Fisica , Universidad Nacional de Colombia, Bogota, Colombia, associated to[10]
[70] Institut für Physik, Universität Rostock, Rostock, Germany, associated to[14]
[71] Van Swinderen Institute, University of Groningen, Groningen, Netherlands, associated to[29]
[72] National Research Centre Kurchatov Institute, Moscow, Russia, associated to[36]
[73] National University of Science and Technology "MISIS", Moscow, Russia, associated to[36]
[74] National Research University Higher School of Economics, Moscow, Russia, associated to[39]
[75] National Research Tomsk Polytechnic University, Tomsk, Russia, associated to[36]
[76] Instituto de Fisica Corpuscular, Centro Mixto Universidad de Valencia — CSIC, Valencia, Spain, associated to[42]
[77] University of Michigan, Ann Arbor, U.S.A., associated to[63]
[78] Los Alamos National Laboratory (LANL), Los Alamos, U.S.A., associated to[63]

[a] Universidade Federal do Triângulo Mineiro (UFTM), Uberaba-MG, Brazil
[b] Laboratoire Leprince-Ringuet, Palaiseau, France
[c] P.N. Lebedev Physical Institute, Russian Academy of Science (LPI RAS), Moscow, Russia
[d] Università di Bari, Bari, Italy
[e] Università di Bologna, Bologna, Italy
[f] Università di Cagliari, Cagliari, Italy
[g] Università di Ferrara, Ferrara, Italy
[h] Università di Genova, Genova, Italy
[i] Università di Milano Bicocca, Milano, Italy
[j] Università di Roma Tor Vergata, Roma, Italy
[k] Università di Roma La Sapienza, Roma, Italy
[l] AGH — University of Science and Technology, Faculty of Computer Science, Electronics and Telecommunications, Kraków, Poland
[m] LIFAELS, La Salle, Universitat Ramon Llull, Barcelona, Spain
[n] Hanoi University of Science, Hanoi, Vietnam
[o] Università di Padova, Padova, Italy
[p] Università di Pisa, Pisa, Italy
[q] Università degli Studi di Milano, Milano, Italy
[r] Università di Urbino, Urbino, Italy

[s] *Università della Basilicata, Potenza, Italy*

[t] *Scuola Normale Superiore, Pisa, Italy*

[u] *Università di Modena e Reggio Emilia, Modena, Italy*

[v] *H.H. Wills Physics Laboratory, University of Bristol, Bristol, United Kingdom*

[w] *MSU — Iligan Institute of Technology (MSU-IIT), Iligan, Philippines*

[x] *Novosibirsk State University, Novosibirsk, Russia*

[y] *Sezione INFN di Trieste, Trieste, Italy*

[z] *School of Physics and Information Technology, Shaanxi Normal University (SNNU), Xi'an, China*

[aa] *Physics and Micro Electronic College, Hunan University, Changsha City, China*

[ab] *Lanzhou University, Lanzhou, China*

[†] *Deceased*